ATOMIC PROCESSES IN GASEOUS NEBULAE

by

ANDRI PROZESKY

submitted in fulfilment of the requirements for the

degree of

MASTER OF SCIENCE

in the subject of

ASTRONOMY

at the

UNIVERSITY OF SOUTH AFRICA

Supervisor: PROF D P SMITS

MAY 2011

Acknowledgements

I owe sincere and earnest thankfulness to my supervisor, Prof. D. P. Smits, without whose encouragement, guidance and support this work would not have been possible.

I wish to express my love and gratitude to my husband, Burr, for his understanding and continued support during stressful times.

I am grateful to Bennie Leonard for his assistance with all things computer related.

The financial assistance of the South African Square Kilometre Array Project towards this research is hereby acknowledged. Opinions expressed and conclusions arrived at, are those of the author and are not necessarily to be attributed to the NRF.

Summary

The atomic physics relevant to gaseous nebulae is critically examined using modelling software with particular emphasis on radio recombination lines (RRLs). The theoretical spectral line intensities can be deduced if we know the population structure of the bound electrons in the gas under non-thermal equilibrium conditions. The population structure of hydrogen is solved for various environments using a capture-collision-cascade model that incorporates an ambient radiation field.

The validity of assuming Case B (Baker & Menzel, 1938) for nebulae is investigated. It is known that Case B is appropriate for levels with small principal quantum numbers ($n < 40$), but this assumption is re-examined for high levels which are relevant to RRLs.

Effects of an ambient radiation field on the population structure is examined and processes that are stimulated by a radiation field are included in the model. This is done as a preliminary investigation to extend the model to a photoionization code.

KEYWORDS: atomic data — atomic processes — line: formation — opacity — plasmas — radiative transfer — ISM: atoms — HII regions — radio lines: ISM

Contents

Chapter 1

Introduction

1.1 Physics of Gaseous Nebulae

The understanding of the physics of ionized gasses is crucial to many subjects in astronomy. Emission spectra can be observed from numerous astronomical objects and the interpretation of these spectra is essential to understand, and scientifically describe them. The study of lines in these spectra has yielded valuable information regarding the most elementary atomic processes occurring in the Universe and has proven to be an essential tool in astronomy.

Gaseous nebulae are often permeated by an external radiation field, generally from a nearby star or stars. The particles (atoms, ions and electrons) in the nebula and the photons of the radiation field interact in such way that the physical properties of the nebula can be deduced by studying the resultant light coming from the plasma. To model the theoretical spectrum that we would expect to see from a specific nebula, it is necessary to have a detailed knowledge of the microscopic processes occurring within the nebula.

When a photon is absorbed by an atom, it induces an upward transition between bound energy states of the atom. If the photon has more energy than the ionization potential of the atom, the valence electron will be liberated from the atom and the excess energy will be converted to kinetic energy of the free electron. The free electrons in gaseous nebulae are mostly liberated by photoionization and collide frequently, setting up a Maxwellian velocity distribution characterized by a temperature T_e (Bohm & Aller, 1947). The distribution of free electrons have temperatures

typically between 5 000 and 20 000 K. The particles in the nebula also interact with each other collisionally, resulting in the excitation, de-excitation and ionization of atoms.

Free electrons in the plasma are continuously being recaptured by ions. If an electron is captured into an excited level of the atom, the electron will cascade to lower energy states through radiative decay and emit photons at very specific frequencies. Emission spectral lines can then be observed at these frequencies. The relative intensities and shapes of these lines provide information about the conditions of the environment where they are formed.

1.2 Radio Recombination Lines

A special class of spectral lines results from transitions between highly excited atomic states. These arise when an electron is captured by an ion into an energy level with a large principal quantum number n. If the downward cascading electron makes transitions between levels with small energy differences, it can produce photons that are in the radio regime. Spectral lines that result from this process that are in the radio regime are referred to as radio recombination lines (RRLs).

The first RRL that was observed was the hydrogen line from principal quantum levels $n_{91} \rightarrow n_{90}$ (H90α) at 8.9 GHz (Sorochenko & Borodzich, 1966). Since then, many more RRLs have been detected, typically involving principal quantum numbers between 60 and 150 for hydrogen. Stepkin et al. (2007) detected carbon lines to levels as high as $n = 1009$ in the direction of Cassiopeia A near 26 MHz. Generally, hydrogen lines where the lower principle quantum number $n_l > 40$ are categorized as RRLs.

The value of radio astronomy has been recognised increasingly in recent years. This is evident in the amount of resources that are being contributed towards the development of new state of the art radio instruments such as the SKA, MeerKAT and ALMA. These new telescopes will open new doors for observational radio astronomy. The new telescopes will have a much greater sensitivity than we have known up to now and this will be especially significant for observations of RRLs. An accurate model for RRLs is essential so that we are able to interpret observations and reap the full benefits of these high-quality measurements.

RRLs have the advantage over their optical counterparts that they are less affected by interstellar extinction and therefore can be detected from very large distances. Working in the radio regime also has the advantage that high spectral resolution can be obtained. This means that individual RRLs can be discerned, even though they have smaller frequency separations than optical lines.

RRLs have proven to be a powerful tool in astronomy. They occur in over five orders of magnitude of wavelengths and subsequently can be observed in objects with vastly different physical parameters. The most obvious application of RRL observations is to deduce the physical properties of the interstellar medium (ISM). The ISM has a very close relationship to stellar formation and death, and to know the conditions of the ISM accurately adds to the understanding of these important processes. About 90 % (by number) of the ISM is made up of hydrogen, with 10 % helium and less than 1 % of metals. RRLs can be observed from various metals; in particular, observations of carbon have proved to be invaluable in the study of the cold ISM.

Several RRL surveys (e.g. Reifenstein et al., 1970; Wilson et al., 1970; Downes et al., 1980; Caswell & Haynes, 1987) have been done to determine the HII distribution within the Galaxy. These observations have facilitated the mapping of large-scale structure of our Galaxy, specifically locating the spiral arms. Besides discrete HII regions, RRLs can also be detected from the diffuse ionized component of the Galaxy that forms a disk close to the Galactic plane.

RRLs have also been detected from extra-galactic sources (e. g. Rodríguez-Rico et al., 2007; Roy et al., 2008, 2010). Currently, it appears that RRL emission is generally from starburst galaxies. RRLs are also expected from quasars and radio galaxies, but these are yet to be detected.

RRLs may prove important for cosmological observations. There has been an increasing interest in the hyperfine transition of neutral hydrogen at 21 cm to study the early Universe, specifically the Epoch of Reionization. Peters et al. (2011) demonstrate that spectral fluctuations from RRLs quite possibly will be comparable to the HI signal and corrupt the data. Therefore, it is of paramount importance to be able to separate the RRLs from the HI signatures, if valuable information is to be extracted from the HI measurements.

RRLs are clearly of great value to a wide variety of topics in astronomy. But to be able to utilize this powerful tool to the fullest, a solid theoretical foundation is

needed to interpret observations. The spectral line fluxes that are observed depend on the occupation number of the quantum states of the atoms or ions in the nebula. Accurate and robust models for the spectral line intensities, and thus the occupation numbers, for the varied conditions under which they form are absolutely essential.

1.3 Objectives and Motivation

The main objective of this work is to develop an independent model for hydrogen plasmas that is applicable to a large portion of the electromagnetic spectrum, in particular to the radio regime. Hitherto, models for gaseous nebulae have focused on transitions at optical and infra-red wavelengths, while the importance of processes involving levels with large principal quantum numbers have not always been recognised. The processes influencing the fluxes of RRLs have become more important as of late with the growing appreciation for the value of radio astronomy. Proper examination of nebulae at radio wavelengths is necessary to understand fully the physics involved in these objects.

Hydrogen is by far the most abundant element in astrophysical environments, and therefore exhaustive understanding of the physics of the processes involved in populating the levels of the hydrogen atom will provide us with a vast amount of information about the Universe. Moreover, the two-body nature of the hydrogen atom allows many of the calculations of the processes to be done analytically. This greatly reduces the uncertainties involved in calculations of the atomic rates compared to calculations for more complex atoms. Complex atoms with a single valence electron in an energy level with a large principal quantum number n can be approximated using a hydrogenic model.

The model simulates the influences of the ionizing radiation, free particle temperature and density on the excited level population structure of hydrogen. From this, the expected spectral line intensities can be calculated. The model considers an unbounded pure hydrogen plasma permeated by an external radiation field.

In order to develop such a model, detailed knowledge of the atomic physics related to astronomical plasmas is required. Calculations of the atomic processes are done at a microscopic level using quantum mechanics. The interactions between the bound electrons of the atoms, the free electrons and protons and the photons in the

ambient radiation field are considered. As few as possible assumptions are made in the calculations to keep the model as accurate as possible. Because of the large number of levels considered, some simplifications are required to be able to do the computations in a reasonable time.

Models to calculate the level populations of hydrogen in gaseous nebulae do exist at present, but they have various shortcomings that affect their applicability to RRLs. Cloudy, XSTAR and a program by Brocklehurst & Salem (1977) are reputable capture-collision-cascade models for nebulae, but these models do not consider very high energy levels ($n > 200$). The definitive hydrogen RRL calculations are presently those of Storey & Hummer (1995) whose calculations go up to $n = 1\,000$. However, they do not take the atomic processes associated with a radiation field into account in these calculations. The importance of processes such as stimulated (bound-bound) emission and stimulated recombination in RRLs needs to be assessed.

Calculations are done for two distinct cases of nebular extinction, namely Case A and Case B (Baker & Menzel, 1938). The distinction between the two situations concerns the treatment of Lyman transitions. Observations at optical wavelengths indicate that Case B calculations are appropriate in this regime. This work shows that the Case B approximation is also appropriate to RRLs.

Another role of this model is to check the results generated by previous models. In the evolution of recombination line modelling, many authors have found numerical errors in preceding work. Bauman et al. (2005) claim that because of the sheer amount of calculations involved in such models, bookkeeping and numerical mistakes are almost unavoidable. They propose that the only way to be sure of the accuracy of results is to compare them with independently-developed code.

The completed model has a lot of potential for further development into a sophisticated code with wide applicability. The code can be expanded to a full photoionization code that includes radiative transfer through the plasma. The hydrogenic model serves as a basis for all other atoms and the model has been written in such a way to facilitate improvements to be added at a later stage.

1.4 Methodology

The spectral line intensities that we observe from nebulae need to be compared to theoretical values in order to determine the physical parameters such as temperature, density and abundances of these objects. The theoretical line intensities can be deduced if we know the populations of the excited states of the atoms in the gas under non-thermal equilibrium conditions. This means that the number density of the bound electrons in every quantum level needs to be known. We can determine this population structure by considering the microscopic processes whereby electrons make transitions between levels that occur in astrophysical gasses.

The particles in the plasma and the photons in the radiation field can interact by means of various atomic processes. All of these processes reach an equilibrium condition called statistical balance, provided that there are no kinematic changes in the gas that are fast enough to compare to the atomic transition rates. This condition can be used to set up balance equations of the processes affecting the populations of each energy level of the atoms. These balance equations are coupled and need to be solved simultaneously to give a factor called the departure coefficient of every energy level. These coefficients are related directly to the occupation number of the level, so the population structure is solved if they are known.

The balance equations are linear with respect to the departure coefficients and a matrix scheme is therefore implemented for their solution. The probability of each atomic process occurring into and out of every energy level needs to be calculated to populate the matrix. Energy levels up to principal quantum number $n \approx 500$ are considered explicitly, with pseudo levels up to $n = 1\,000$.

The solution for the departure coefficients can be given only for distinct energy levels of the atoms, known as an n-model, or angular momentum states can be resolved and a departure coefficient calculated for every angular momentum state, called an nl-model. In this work, an n-modelwas developed. This is appropriate for RRLs, since the angular momentum states of the highly excited levels are statistically populated according to their statistical weights, and direct calculation of the individual departure coefficients of the angular momentum states is not necessary.

The model was coded in the programming language C using the MinGW compiler on a Windows XP platform. The code was written completely independently using algorithms described in literature, as discussed in the relevant chapters. No

existing codes were copied but the results were checked against models written in FORTRAN (Smits, private communication). Some of the C programs were run on other platforms (in particular, Linux) at various stages of development of the code, and produced identical results to those described here. Therefore, the code appears to be robust across platforms and machines.

1.5 Overview

Chapter 2 is an overview of the atomic theory involved in a model of gaseous nebulae. The atomic processes that occur in recombination plasmas and the determination of their transition probabilities are discussed in detail. Both radiative and collisional transitions between bound energy states of the atom and between a bound state and the continuum are reviewed. An overview of the quantum mechanics of electrons making energy transitions in a Coulomb field is also presented.

Chapter 3 formulates how the atomic rates are utilized to determine the level populations of the atomic energy levels. The concept of the departure coefficient is introduced, which is central to the model. A summary of the history and evolution of departure coefficient calculations is given.

The computational details of the rates of the atomic processes discussed in Chapter 2 is presented in Chapter 4. The methods used in this work, and some tests to establish their validity, are referenced and discussed thoroughly.

Numerical methods are necessary in most codes, since computing power is finite. Chapter 5 deals with the numerical methods implemented in this model to economise memory use and speed up calculations.

The results of the model are presented in Chapter 6. The determined departure coefficients are compared to previous calculations and a preliminary investigation into the effect of an external radiation field is given.

Chapter 7 looks at the applicability of an assumption that significantly influence the departure coefficients under various conditions. An investigation is done on the escape probability of Lyman photons from astronomical plasmas, to see when transitions from and to the ground state of atoms should be disregarded.

Chapter 8 provides a discussion on the work presented here and future work that will be done on this project is discussed.

Chapter 2

Atomic Processes

Detailed knowledge of the individual atomic processes that are important in gaseous nebulae are required to determine the level populations of the atoms. When matter and radiation interact, photons are removed or added to the radiation field by various processes that change the internal energy of atoms. This chapter addresses the theoretical aspects of these processes. Calculational details regarding the rates of the atomic processes are discussed in Chapter 4. The microscopic processes can be categorized as radiative transitions between bound states, radiative transitions between bound states and the continuum, and transitions induced by collisions with free particles. Collisional transitions also occur between two bound states, or a bound and a free state. Electron collisions are much more effective than proton collisions in energy-changing collision (Brocklehurst, 1970), therefore only collisions with electrons will be considered in this work.

2.1 Bound-Bound Radiative Processes

2.1.1 Spontaneous Emission

Bound electrons in excited energy levels can decay spontaneously to lower energy levels. To conserve the energy of the system, a photon is radiated away in an arbitrary direction with energy $h\nu$, equal to the energy difference between the two bound levels. Consider a spontaneous emission transition from an upper energy level

n to a lower level n'. The reaction can be represented by

$$X_n \rightarrow X_{n'} + h\nu \,.$$

These transitions occur at a rate of $A_{nn'}\,\mathrm{s}^{-1}$ where $A_{nn'}$ is the spontaneous emission rate referred to as the Einstein A-value.

For a gas where N_n and $N_{n'}$ are the populations for levels n and n' respectively, the level populations would change due to spontaneous emissions according to

$$-\frac{dN_n}{dt} = \frac{dN_{n'}}{dt} = N_n A_{nn'} \,.$$

The transition rate can also be resolved to incorporate transitions to and from individual angular momentum states in the energy levels. The probability of a spontaneous transition from a level nl to level $n'l'$ is $A_{nl,\,n'l'}$. The total probability for a spontaneous transition from level n to level n' can be calculated from the $A_{nl,\,n'l'}$ by summing over the angular momentum states and weighting the $A_{nl,\,n'l'}$ according to the statistical weights of the individual angular momentum states. For allowed dipole transitions, this is

$$A_{nn'} = \frac{1}{n^2} \sum_{l} \sum_{l'=l\pm1} (2l+1)\, A_{nl,\,n'l'} \,.$$

2.1.2 Absorption

An electron initially in level n' can make an upward transition to a higher level n by absorbing a photon from an ambient radiation field,

$$X_{n'} + h\nu \rightarrow X_n \,.$$

The rate of absorption transitions is

$$\frac{dN_n}{dt} = -\frac{dN_{n'}}{dt} = N_{n'} B_{n'n} J_\nu$$

where J_ν is the mean intensity of the external radiation field.

Einstein (1916) derived general relations between the rates of the bound-bound radiative processes. He showed that the probability of absorption can be written in terms of the probability of a spontaneous emission as

$$B_{n'n} = \frac{g_n}{g_{n'}} \frac{c^2}{2h\nu^3} A_{nn'} = \left(\frac{n}{n'}\right)^2 \frac{c^2}{2h\nu^3} A_{nn'} \tag{2.1.1}$$

where g_k is the degeneracy of level k.

2.1.3 Stimulated Emission

In the presence of a radiation field an electron can be stimulated to make a downward transition, emitting a photon with the same frequency as the stimulating photon,

$$X_n + h\nu \rightarrow X_{n'} + h\nu + h\nu \,.$$

The rate of change of the level populations due to stimulated emission is

$$-\frac{dN_n}{dt} = \frac{dN_{n'}}{dt} = N_n B_{nn'} J_\nu$$

where J_ν is the mean intensity of the stimulating radiation field.

Stimulated emission is the inverse process to absorption and is often included as a negative absorption. The process of stimulated emission is only important when the Rayleigh-Jeans condition holds ($h\nu \ll kT$).

Einstein (1916) showed that the stimulated emission coefficient $B_{nn'}$ is related to the absorption coefficient $B_{n'n}$ and the spontaneous emission coefficient $A_{nn'}$ by

$$B_{nn'} = \frac{g_{n'}}{g_n} B_{n'n} = \frac{c^2}{2h\nu^3} A_{nn'} \,. \tag{2.1.2}$$

2.2 Bound-Free Radiative Processes

2.2.1 Radiative Recombination

Radiative recombination is the process whereby an ion captures a free electron into a bound state with the excess energy being radiated away as a photon. If the electron

is captured into an excited state of the atom, it will decay to the ground state by a number of radiative transitions. Let $X^{+(i)}$ be an i-times ionized atom, $X_n^{+(i-1)}$ has a valence electron in the state n. In the case of hydrogen, $X^{+(i)}$ is just the bare nucleus, a proton. Radiative recombination is given by

$$X^{+(i)} + e^- \rightarrow X_n^{+(i-1)} + h\nu\,.$$

The energy of the system has to be conserved, so the kinetic energy of the free electron and the energy of the emitted photon are related by

$$h\nu = \chi_n + \frac{1}{2} m_e v^2 \tag{2.2.1}$$

where χ_n is the ionization potential of the level n of the atom, m_e is the mass of the electron and v is the free electron speed. The probability of a radiative recombination increases as the the velocity between the free electron and ion becomes smaller.

The radiative recombination rate to a level n per unit volume is dependent on the cross-section for radiative recombination, $\sigma_n^r(v)$, for an electron with a velocity v. The total recombination rate coefficient α_n^r is found by averaging the cross-section over the velocity distribution function $f(v)$ of the free electrons. The recombination rate also depends on the number densities of the free electrons and the ions, N_e and N_i respectively, and is given by

$$N_e N_i \int \sigma_n^r(v) v f(v)\, dv = N_e N_i \alpha_n^r\,. \tag{2.2.2}$$

Bohm & Aller (1947) showed that in gaseous nebulae, collisions amongst the free electrons set up a Maxwellian distribution for these particles on time scales that are much shorter than other atomic processes. Therefore, it is appropriate to use a Maxwellian distribution which is given by

$$f\,(v)\; dv = 4\pi v^2 \left(\frac{m_e}{2\pi k_B T_e}\right)^{3/2} e^{-m_e v^2/(2k_B T_e)}\, dv\,,$$

to describe the velocity distribution of the free electrons, where k_B is the Boltzmann constant and T_e is the free electron temperature.

2.2.2 Photoionization

Photoionization is analogous to the bound-bound process of absorption. This process involves a bound electron of an atom being liberated to the continuum due to the absorption of a photon,

$$X_n^{+(i-1)} + h\nu \rightarrow X^{+(i)} + e^- \,.$$

The ionizing photon has to have a higher energy, and thus higher frequency, than one involved in a bound-bound absorption reaction from the same level, as the incoming photon has to have sufficient energy to lift the electron to a free state, as descibed by (2.2.1).

The rate of photoionizations out of bound level n of a atom or ion per unit volume will depend on the number density N_n of atoms or ions in the state n. For a plasma in an ambient radiation field with mean intensity J_ν, the number of photons in the frequency interval ν to $\nu + d\nu$ that can ionize an atom is $4\pi J_\nu d\nu/(h\nu)$. Only photons with energies higher than χ_n will be able to ionize an electron from state n. Let $a_n^p(\nu)$ be the photoionization cross-section from level n for a photon with frequency ν, then the rate of photoionizations per unit volume is given by

$$N_n \int_{\chi_n/h}^{\infty} a_n^p(\nu) \frac{4\pi J_\nu}{h\nu} \, d\nu = N_n \alpha_n^p \,. \tag{2.2.3}$$

2.2.3 Stimulated Recombination

A free electron can be stimulated by a photon from the ambient radiation field to recombine to a bound level of an ion with a processes analogous to stimulated emission

$$X^{+(i)} + e^- + h\nu \rightarrow X_n^{+(i-1)} + h\nu + h\nu \,.$$

Let $\sigma_n^s(v)$ be the cross-section for stimulated recombination of an electron with a speed v into level n. To obtain the total rate of stimulated recombination, the cross-section needs to be averaged over the free electron velocity distribution, as the chances of a stimulated recombination depends on the velocity of the recombining electron. For a radiation field with mean intensityJ_ν the number of photons that

can stimulate such a recombination is $4\pi J_\nu \, d\nu/(h\nu)$. The speed of the free electron and the frequency of the emitted photon are related by (2.2.1). This leads to $dv = h/(mv)\, d\nu$. Putting all of this together gives the rate at which stimulated recombinations occur as

$$N_e N_i \int_{\chi_n/h}^{\infty} \frac{4\pi J_\nu}{h\nu} \sigma_n^s(v)\, f(v) \frac{h}{m}\, d\nu = N_e N_i \alpha_n^s \,. \tag{2.2.4}$$

2.3 Collisional Transitions

2.3.1 Bound-Bound Transitions

An unbound electron may interact with a bound electron, causing the bound electron to make a transition from one energy level to another. The free electron will either absorb or transfer energy to the bound electron in such a way that the kinetic energy of the free electron changes to conserve the energy of the system. The processes of collisional excitation and de-excitation are given by

$$X_n + e_E^- \leftrightarrows X_{n'} + e_{E'}^- \,.$$

Let n and n' be two principle quantum numbers representing atomic energy levels with $n > n'$. The cross-section for such an excitation $\sigma_{n'n}$ is a function of the free electron's velocity v and is zero if the electron's energy is below $E_{n'n} = h\nu_{n'n}$.

Because their mass is very small compared to other free particles in the plasma, electrons usually dominate energy-changing collisions. This means that their speeds are much larger than those of other free particles and leads to a stronger perturbation to the wave functions of bound electrons than a slower interaction with a more massive particle would.

The collisional excitation rate coefficient $C_{n'n}$ is obtained by averaging the cross-section over the velocity distribution, that is

$$C_{n'n} = \int \sigma_{n'n}(v)\, v f(v)\, dv$$

where $f(v)$ is the free electron distribution function.

The collisional excitation rate per unit volume per unit time depends on the number density of the free electrons and the atoms in the initial state n' and is given by

$$N_e N_{n'} C_{n'n} \, .$$

For a system in TE at temperature T, the level populations will follow a Boltzmann distribution

$$\frac{N_n}{N_{n'}} = \frac{g_n}{g_{n'}} e^{-(E_n - E_{n'})/k_B T} \, . \tag{2.3.1}$$

where g_k is the statistical weight of level k and k_B is the Boltzmann constant. Let $C_{nn'}$ be the collisional de-excitation rate. The principle of detailed balance requires that

$$N_n C_{nn'} = N_{n'} C_{n'n}$$

in TE. Substituting (2.3.1) for $N_{n'}/N_n$ in the above equation yields a relationship between the coefficients for excitation and de-excitation which is given by

$$C_{nn'} = \frac{g_{n'}}{g_n} e^{-(E_{n'} - E_n)/k_B T} C_{n'n} = \left(\frac{n'}{n} \right)^2 e^{-(E_{n'} - E_n)/k_B T} C_{n'n} \, . \tag{2.3.2}$$

2.3.2 Bound-Free Transitions

If a colliding electron has sufficient energy when it interacts with a bound electron, it can liberate a bound electron to the continuum by a process called collisional ionization. Collisional ionization is given by the forward reaction in

$$X^{+(i-1)} + e^-_E \leftrightarrows X^{+(i)} + e^-_{E'} + e^-_{E''} \, .$$

The backward reaction represents the inverse process of collisional ionization, namely three-body recombination.

The collisional ionization rate coefficient out of level n, C_{ni}, is given by the collisional ionization cross-section, σ_{ni}, for a bound level n by a free electron with velocity v, averaged over the free electron distribution distribution function so that

$$C_{ni} = \int \sigma_{ni}(v) \, v f(v) \, dv \, .$$

The collisional excitation rate per unit volume per unit time depends on the number

density of the free electrons and the atoms in the initial state n and is given by $N_e N_n C_{ni}$. Because three-body recombination requires two free electrons and an ion, the rate is $N_e^2 N_i C_{in}$.

The Saha-Boltzmann equation relates the number density of atoms in level n to the number density of the free electrons N_e and ions N_i present in a gas in TE at temperature T

$$\frac{N_n}{N_e N_i} = \frac{g_n}{g_e g_i} \left(\frac{h^2}{2\pi m_e k_B T} \right)^{3/2} e^{\chi_n / kT} . \tag{2.3.3}$$

The degeneracy of level n of a hydrogenic ion or atom is $g_n = 2n^2$ and the degeneracy of an electron $g_e = 2$ to account for the two possible spin states of an electron. For hydrogen, the degeneracy of the proton g_i is taken as 1. The proton spin serves a as reference, with the spin of an electron being either parallel or anti-parallel to the proton spin.

In TE the principle of detailed balance requires that

$$N_e N_n C_{ni} = N_e^2 N_i C_{in} .$$

Using the Saha-Boltzmann equation to relate N_e, N_i and N_n for hydrogen, this gives

$$n^2 e^{\chi_n / kT_e} C_{ni} = \left(\frac{2\pi m_e k T_e}{h^2} \right)^{3/2} C_{in} .$$

2.4 Quantum Mechanics of Atomic Transitions

To be able to calculate the rates of transitions between two quantum mechanical states, the wave functions of both states need to be known. The time-independent (non-relativistic) Schrödinger equation for a one-electron atom with a nuclear charge Z in a Coulomb potential can be solved explicitly. Because the potential is spherically symmetric, the eigenfunctions ψ_{nlm} can be separated into a radial $R_{nl}(r)$ and angular part $Y_{lm}(\theta, \phi)$ of the form

$$\psi_{nlm} = R_{nl}(r)\, Y_{lm}(\theta, \phi) \tag{2.4.1}$$

where m is the magnetic quantum number. The eigenvalues for the energy are given by

$$E_{nl} = -\frac{Z^2 e^2}{2 a_0 n^2}$$

where a_0 is the Bohr radius. Note that the energy is degenerate with respect to l for a Coulomb field.

In the presence of an ambient radiation field, an electromagnetic perturbation can lead to transitions from one stationary state to another. It is this perturbation that will cause electrons to make transitions from one state to another. An approximation to the perturbation can be made called the electric dipole approximation. Under this approximation only the strongest transitions, called electric dipole transitions, are taken into account. Electric dipole transitions have higher rates than other transitions, so this is a sound assumption under most circumstances.

By Fermi's golden rule, and assuming the electric dipole approximation, the probability of an electron making a transition from an eigenstate $|\psi_i\rangle$ to another state $|\psi_f\rangle$ depends on the quantity

$$\langle\psi_i|\,\mathbf{r}\,|\psi_f\rangle = \int R_i r R_f\, dr \int Y_i Y_f\, d\Omega \tag{2.4.2}$$

where $d\Omega = \sin\theta\, d\theta\, d\phi$ and the integrals are over all space.

The angular integral can be evaluated explicitly and restricts the change of the angular momentum quantum number for the transition so that for an electric dipole transition $\Delta l = \pm 1$. Transitions that obey this selection rule are called allowed transitions.

The quantity

$$\tau_i^f = \int_0^\infty R_i\, r\, R_f\, dr$$

is called the radial dipole matrix element. The evaluation of this radial integral can be arithmetically tedious and transition probabilities are often written in terms of this quantity.

The Bethe theory (Inokuti, 1971) describes inelastic collisions between fast charged particles, like electrons, and ions or atoms. The theory relates the cross-sections, and therefore the rate coefficients, of the bound-bound collisional processes to the quantity τ_i^f. Clearly, the radial matrix element plays a significant role in the determination of the rates of various atomic processes.

The next chapter will discuss the level populations of atoms in the ISM. Methods of computing the rates of individual atomic processes and radial matrix elements will be discussed in Chapter 4.

Chapter 3

Atomic Level Populations

Radiation from astronomical objects carries a large amount of information regarding the source. As the light travels through the ISM, the particles of the ISM imprint information about the characteristics of the ISM on the radiation as well. The properties of the source object, as well as the ISM that the photons have traveled through can then be deduced from the characteristics of the observed radiation.

One of the main ways in which we can extract the information from the radiation is to interpret its spectrum, where emission and absorption lines are distinct features. The intensities of these spectral lines are a rich source of information regarding the physical characteristics of the ISM and the source object. To be able to interpret the emission and absorption spectrum, we need to know the population structure of the electrons in excited states of the constituent atoms of the source and the ISM.

The level populations of states within an atom or ion would follow a Boltzmann distribution (2.3.1) if the system were in TE. However, astrophysical plasmas are in general not in TE, but Menzel (1937) introduced a very elegant method for expressing departures from TE in gaseous nebulae (see § 3.1) which is adopted in this work.

Kardashev (1959) first suggested the possibility of detecting recombination lines at radio wavelengths. He argued that the departures from TE for levels with large principal quantum numbers is so small, that Boltzmann distributions may be assumed when working with RRLs. However, Goldberg (1966) showed that very small deviations from the Boltzmann distribution are indeed important at radio wavelengths and affect calculated line intensities notably.

3.1 Departure Coefficients

A system is said to be in thermodynamic equilibrium (TE) if the energy exchange between all its components is so rapid that all components can be described by a single parameter, namely the temperature T. TE is an idealization that is generally not found in the open systems that occur in astronomical environments. There are situations where TE may be used as an approximation locally. Such systems are said to be in local thermodynamic equilibrium (LTE).

Menzel (1937) introduced a correction factor b_n to compensate for the degree of departure from LTE of the level population. In this scheme, the Saha-Boltzmann equation (2.3.3) becomes

$$N_n = b_n N_e N_i \left(\frac{h^2}{2\pi m_e k_B T_e} \right)^{3/2} n^2 \exp\left(\frac{\chi_n}{k_B T} \right) . \tag{3.1.1}$$

The b_n factors are called departure coefficients and b_n equal to unity indicates strict TE. The level populations of a gas described by a specific electron temperature T_e and electron density N_e are solved if the departure coefficients for all levels are known.

The Boltzmann equation (2.3.1) also changes for non-LTE conditions. For $m > n$ the relative populations of bound levels are described by

$$\frac{N_m}{N_n} = \frac{b_m}{b_n} \frac{g_m}{g_n} e^{-h\nu/k_B T_e} = \frac{g_m}{g_n} e^{-h\nu/k_B T_{ex}} . \tag{3.1.2}$$

Here T_e is the free electron temperature and T_{ex} is the excitation temperature which is a parameter that describes the relative populations of bound quantum levels. The excitation temperature is an alternative way of expressing population deviations and is often used in radio astronomy.

The rates of the atomic processes are much faster than dynamical changes in the plasma, hence it is appropriate to assume that the plasma is stationary over time-scales that we observe it. For this reason the level populations are described by statistical equilibrium. This means that all transitions into any particular atomic level n must equal the transitions out of level n. Hence

$$\sum_{\substack{m \\ n \neq m}} N_n P_{nm} = \sum_{\substack{m \\ n \neq m}} N_m P_{mn} \tag{3.1.3}$$

where P_{ij} is total rate of transitions from level i to level j. It should be noted that statistical equilibrium is a less stringent condition than LTE. In LTE (or TE) it is necessary that every process is exactly balanced by the same kind of process, also called the principle of detailed balance. Statistical equilibrium only requires the total rate of all processes to balance for every level.

It should be noted that even though an entire system is not in TE, some of its components may be in TE. For a plasma, the free electrons can be described by a Maxwellian distribution defined by a single temperature T_e and the radiation field can have a blackbody spectrum with a temperature T_r, but the two components will not be in equilibrium with each other unless $T_e = T_r$.

The departure coefficients for atoms in a plasma can be calculated by setting up rate equations like (3.1.3) for every energy level and solving the system of equations simultaneously. Therefore, it is necessary to have detailed knowledge of all the microscopic processes occurring within the nebula. Large scale effects are not considered in this work, and I assume that conditions can be specified locally.

Assembling all the atomic processes occurring into and out of level n as required by (3.1.3), gives the statistical balance equation

$$\begin{aligned} & N_e N_i \left(\alpha_n^r + \alpha_n^s + N_e C_{i,n}\right) + \sum_{m>n} N_m \left(A_{mn} + N_e C_{mn} + B_{mn} J_\nu\right) \\ & \qquad + \sum_{k<n} N_k \left(N_e C_{kn} + B_{kn} J_\nu\right) \qquad (3.1.4) \\ = \; & N_n \left[\alpha_n^p + N_e C_{n,i} + \sum_{k<n} \left(A_{nk} + N_e C_{nk} + B_{nk} J_\nu\right) + \sum_{m>n} \left(N_e C_{nm} + B_{nm} J_\nu\right)\right]. \end{aligned}$$

The left-hand side contains all processes that populate level n. The terms represent radiative recombination, stimulated recombination, three-body recombination, spontaneous emission, collisional de-excitation, stimulated emission, collisional excitation and absorption, respectively.

The right-hand side includes all processes that depopulate level n. The terms represent photoionization, collisional ionization, spontaneous emission, collisional de-excitation, stimulated emission, collisional excitation and absorption, respectively.

J_ν is the mean intensity of the incident radiation field. In this work the electron number density N_e and the ion number density N_i are uncoupled from the bound level populations N_n and are taken as constant throughout the plasma.

The departure coefficients b_n are related to the number density N_n of atoms in level n through (3.1.1). Substituting this into the rate equation (3.1.4) yields

$$\begin{aligned}
&\left(\frac{2\pi m_e k_B T}{h^2}\right)^{3/2} (\alpha_n^r + \alpha_n^s + N_e C_{i,n}) + \sum_{m>n} b_m m^2 e^{\chi_m/k_B T} \\
&\qquad \times (A_{mn} + N_e C_{mn} + B_{mn} J_\nu) + \sum_{k<n} b_k k^2 e^{\chi_k/k_B T} (N_e C_{kn} + B_{kn} J_\nu) \\
= \; & b_n n^2 e^{\chi_n/k_B T} \left[\alpha_n^p + N_e C_{n,i} + \sum_{k<n} (A_{nk} + N_e C_{nk} + B_{nk} J_\nu) \right. \\
&\left. + \sum_{m>n} (N_e C_{nm} + B_{nm} J_\nu) \right] . \qquad (3.1.5)
\end{aligned}$$

Equation (3.1.5) can be written in matrix form as

$$\mathbf{a} = \mathbf{b} \cdot \mathbf{X}$$

where the row vector $\mathbf{a}$ has components

$$\mathrm{a}_n = \left(\frac{2\pi m_e k_B T}{h^2}\right)^{3/2} (\alpha_n^r + \alpha_n^s + N_e C_{i,n}) \qquad (3.1.6)$$

and the row vector $\mathbf{b}$ has components b_n, $n = 1, 2, 3 \ldots$.

The matrix $\mathbf{X}$ has diagonal entries

$$\mathrm{X}_{nn} = n^2 e^{\chi_n/k_B T} \left[\alpha_n^p + N_e C_{n,i} + \sum_{k<n} (A_{nk} + N_e C_{nk} + B_{nk} J_\nu) + \sum_{m>n} (N_e C_{nm} + B_{nm} J_\nu) \right]$$

which represent all the processes depopulating level n.

Below the diagonal ($m > n$), the matrix elements are given by

$$\mathrm{X}_{mn} = -m^2 e^{\chi_m/k_B T} (A_{mn} + N_e C_{mn} + B_{mn} J_\nu)$$

and above the diagonal ($k < n$) they are

$$\mathrm{X}_{kn} = -k^2 e^{\chi_k/k_B T} (N_e C_{kn} + B_{kn} J_\nu) \; .$$

The non-diagonal matrix elements represent all the processes populating level n. All the processes involving downward transitions into n from higher levels are above the

diagonal and the processes populating n from lower levels are below the diagonal.

The departure coefficients b_n can be obtained by inverting the matrix $\mathbf{X}$ and multiplying it with vector $\mathbf{a}$ from the left, i.e.

$$\mathbf{b} = \mathbf{a} \cdot \mathbf{X^{-1}} \, .$$

The elements of $\mathbf{a}$ and $\mathbf{X}$ depend on the electron temperature T_e, the density N_e, the external radiation field J_ν, and the rates of the individual atomic processes.

3.2 Evolution of Departure Coefficient Calculations

The development of the study of the population structure of hydrogen has been very dependent on computational capabilities. The first calculations for the emission spectrum produced by nebulae were done by Plaskett (1928). He did the calculation assuming a finite number of energy levels and the angular momentum levels were populated statistically according to

$$N_{nl} = N_n \frac{2l+1}{n^2} \, .$$

This is known as an n-model, as opposed to an nl-model where the N_{nl} are calculated explicitly.

Menzel (1937) introduced the concept of the departure coefficient and Baker & Menzel (1938) calculated b_n values using an iterative method. They assumed that the atomic levels are populated by radiative recombination and depopulated only by spontaneous radiative transitions to lower levels. An infinite number of energy levels were accounted for and departure coefficients were given for $n \leq 30$. They used approximations to calculate the Einstein A-values, rather than fully quantum mechanical formulae.

The accuracy of the departure coefficients were improved by Seaton (1959), who introduced an elegant cascade matrix technique and accounted for transitions by all possible routes. Seaton (1964) included transitions between adjacent levels (i.e. $n \rightarrow n \pm 1$) caused by collisions due to free electrons in his calculations, and found that the collisional processes become important when determining the departure coefficients of levels with $n \gtrsim 40$.

Up until this time, the aim of these calculations was to understand the intensities of optical spectral lines in astronomical environments whose lines involve transitions between levels with small values of the principal quantum number n. Following the detection of RRLs (Sorochenko & Borodzich, 1966), the emphasis of the studies shifted to extending the calculations to higher energy levels.

Hoang-Binh (1968) included collisional transitions not only from adjacent levels but from levels with $\Delta n = |n - n'| = 1, 2, 3$. Sejnowski & Hjellming (1969) extended calculations of b_n up to $n = 260$ and considered collisional transitions up to $\Delta n = 20$. Brocklehurst (1970) made authoritative calculations by allowing for radiative and collisional transitions from and to all levels. He also used a matrix condensation technique developed by Burgess & Summers (1969) (see § 5.2) that made it possible to account for a large number of energy levels with the computing power available at the time. Brocklehurst (1971) extended his calculations to an nl-model by considering collisional redistribution of angular momentum.

A very important improvement in calculations was made by Brocklehurst & Salem (1977) and Salem & Brocklehurst (1979) who included the effects of an external radiation field and therefore considered stimulated transitions in n-models. Storey & Hummer (1995) performed accurate calculations and resolved the angular momentum levels, but they did not take the effects of an external radiation into account. The results of Salem & Brocklehurst (1979) and Storey & Hummer (1995) are considered to be the most authoritative at present for hydrogen.

Chapter 4

Atomic Calculations

The calculation of the rates of the various atomic processes relevant to gaseous nebulae are central to the determination of the population structure of atoms in the gas. This chapter deals with the details of how these calculations are implemented in a computer. As described in § 2.4, the radial dipole matrix element plays a fundamental role in the computation of atomic rates. The calculation of the radial matrix elements for the bound-bound and bound-free cases will be described first, followed by the calculational details for the radiative bound-bound processes, the radiative bound-free processes and finally the collisional processes will be looked at.

4.1 Bound-Bound Radiative Processes

4.1.1 Radial Dipole Matrix Elements

As discussed in § 2.4, the radial dipole matrix element τ_i^f contains the quantum mechanical information related to a bound electron in a Coulomb field making a transition from an initial level i to a final level f. Suppose an electron makes a transition between two bound states nl and $n'l'$, with $n > n'$. The dipole radial matrix element for such a transition, $\tau_{nl}^{n'l'}$, is given by

$$\tau_{nl}^{n'l'} = \tau_{n'l'}^{nl} = \int_0^\infty R_{n'l'}\, r\, R_{nl}\, dr$$

where R_{nl} is the normalized radial wave function for the electron state nl. Note the symmetry between the matrix elements for a transition from $nl \rightarrow n'l'$ and its reverse from $n'l' \rightarrow nl$.

Gordon (1929) gives an explicit formula for the bound-bound matrix element of a transition between nl and $n'\,l-1$ for hydrogen as

$$\begin{aligned}\tau_{nl}^{n'\,l-1} &= \frac{2^{2l}}{(2l-1)!}\left[\frac{\Gamma(n+l+1)\Gamma(n'+l)}{\Gamma(n-1)\Gamma(n'-l+l)}\right]^{1/2}(nn')^{l+1}\,(n+n')^{-n-n'}\,(n-n')^{n-l-2} \\ &\quad\times(n'-n)^{n'-l}\left\{{}_2F_1\left[l+1-n,\,l-n',\,2l,\,\frac{-4nn'}{(n-n')^2}\right]\right. \\ &\quad\left.-\,{}_2F_1\left[l-1-n,\,l-n',\,2l,\,\frac{-4nn'}{(n-n')^2}\right]\right\}. \qquad (4.1.1)\end{aligned}$$

where ${}_2F_1$ is the Gaussian hypergeometric function. The matrix element $\tau_{nl}^{n'\,l+1}$ for a transition from $nl \rightarrow n'\,l+1$ is obtained by making the replacements $n \rightarrow n'$ and $l \rightarrow l+1$ in the above formula.

4.1.2 Calculation of A-Values

The rate coefficient of spontaneous emission transitions in a hydrogenic atom is given by (Brocklehurst, 1971)

$$A_{nl,\,n'l'} = \frac{64\pi^4\nu^3}{3Z^2hc^3}\frac{\max(l,\,l')}{2l+1}e^2a_0^2\left[\tau_{nl}^{n'l'}\right]^2$$

in cgs units. In the above expression a_0 is the Bohr radius and ν, the frequency associated with the transition, is given by

$$\nu = cR_HZ^2\left(\frac{1}{n'^2}-\frac{1}{n^2}\right) \qquad (4.1.2)$$

where R_H is the Rydberg constant for a hydrogenic atom with a nucleus that has charge Z.

If μ and m_e are the reduced and rest mass of an electron respectively, and R_∞ is the Rydberg constant for a nucleus with infinite mass, then R_H for an atom with a nucleus of mass M is given by

$$R_H = \frac{\mu}{m_e}R_\infty \quad \text{where} \quad \mu = \frac{m_eM}{m_e+M}\,.$$

Direct calculation of the matrix elements using (4.1.1) is impractical for large principal quantum numbers in double precision due to overflow errors in the calculation of the hypergeometric functions. The matrix elements for $n \leq 500$ were calculated using *Mathematica*[1] and written to a data file that was read from the main program. *Mathematica* can do calculations to a much larger precision than C and gives results exactly as double precision numbers.

For very high energy levels ($n > 500$), the approximation (Brocklehurst, 1970)

$$A_{nm} = \frac{16\alpha^4 c}{3\pi\sqrt{3}a_0} \frac{g_{nm}}{n^3 m \left(n^2 - m^2\right)} \tag{4.1.3}$$

was used, where α is the fine structure constant, a_0 is the Bohr radius and g_{nm} is the bound-bound Gaunt factor given by Baker & Menzel (1938) as

$$g_{nm} = 1 - \frac{0.1728\left(1 + m^2/n^2\right)}{\left(1 - m^2/n^2\right)^{2/3}\left(m\right)^{2/3}}\,.$$

The relative error between values for A-values calculated with (4.1.3) and (4.1.1) is generally less than 1 % for $m > 500$. The error is larger when n is small or when $m - n$ is small. The largest error is 28 %. For such high n levels, the collisional processes are more important than the radiative processes and set up Boltzmann distributions for the level populations resulting in $b_n = 1$. Therefore the errors in the A-values for high n levels do not affect results.

The rate coefficients for absorption and stimulated emission were calculated using the Einstein relations (2.1.1) and (2.1.2), respectively.

4.2 Bound-Free Radiative Processes

4.2.1 Radial Dipole Matrix Elements

The matrix element for a transition between a bound level and a free state can be obtained by analytic continuation of (4.1.1) by letting $n' \to i\eta$. Karzas & Latter (1961) found an expression for the matrix element $\tau_{nl}^{\kappa l'}$ for a transition between bound

[1] *Unisa license number L3300-9097*

level nl and a free state $\kappa l'$ where $\kappa = 1/\eta$ so that the energy difference between the states is given by

$$\begin{aligned} h\nu &= \left(\frac{1}{n^2} - \frac{1}{(i\eta)^2}\right)\chi_n \\ &= \left(1 + n^2\kappa^2\right)\chi_n \end{aligned} \tag{4.2.1}$$

where $\chi_n = Z^2\chi_0/n^2$ is the ionization energy of level n.

Burgess (1965) gives an explicit expression for $\tau_{nl}^{\kappa l'} = g\left(n,\, l;\, \kappa,\, l' = l \pm 1\right)$ as

$$\begin{aligned} g\left(n,\, l;\, \kappa,\, l' = l \pm 1\right) &= \frac{\exp\left[-2/\kappa \arctan\left(n\kappa\right)\right]}{4n^2\left(2l \pm 1\right)!}\left(\frac{4n}{1 + n^2\kappa^2}\right)^{\min(l,l')+1} \\ &\times \left[\frac{\pi}{2}\frac{(n+l)!}{(n-l-1)!\left[1 - \exp\left(-2\pi/\kappa\right)\right]}\prod_{s=0}^{l'}\left(1 + s^2\kappa^2\right)\right]^{1/2} Y_{\pm} \end{aligned} \tag{4.2.2}$$

where

$$\begin{aligned} Y_+ &= i\eta\left(\frac{n - i\eta}{n + i\eta}\right)^{n-l}\left[{}_2F_1\left(l + 1 - n,\, l - i\eta,\, 2l + 2,\, \frac{-4ni\eta}{(n - i\eta)^2}\right)\right. \\ &\left. - \left(\frac{n + i\eta}{n - i\eta}\right)^2 {}_2F_1\left(l + 1 - n,\, l + 1 - i\eta,\, 2l + 2,\, \frac{-4ni\eta}{(n - i\eta)^2}\right)\right] \end{aligned}$$

and

$$\begin{aligned} Y_- &= \left(\frac{n - i\eta}{n + i\eta}\right)^{n-l-1}\left[{}_2F_1\left(l - 1 - n,\, l - i\eta,\, 2l,\, \frac{-4ni\eta}{(n - i\eta)^2}\right)\right. \\ &\left. - \left(\frac{n + i\eta}{n - i\eta}\right)^2 {}_2F_1\left(l + 1 - n,\, l - i\eta,\, 2l,\, \frac{-4ni\eta}{(n - i\eta)^2}\right)\right]. \end{aligned}$$

Because the hypergeometric series all have a finite number of terms, the electric dipole moment matrix elements for bound-free transitions can be computed from (4.2.2) directly . However, because of the large number of terms that can occur in these series, especially for large n and small l, this procedure is not suitable in general.

A method that is based on a set of recurrence relations that is more suitable for computational implementation has been described by Burgess (1965). He set up recurrence relations satisfied by the exact matrix elements for hydrogenic atoms

or ions. These simple recurrence relations allow for fast computing to very high accuracy. The rest of this section will describe the method of Burgess (1965).

Rather than compute the $g(n,\, l;\, \kappa,\, l')$ in (4.2.2), it is more convenient to compute the quantities $G(n,\, l;\, \kappa,\, l')$ which are defined by

$$g(n,\, l;\, \kappa,\, l') = \sqrt{\frac{(n+l)!}{(n-l-1)!}\prod_{s=0}^{l'}\left(1+s^2\kappa^2\right)}\,(2n)^{l-n}\,G(n,\, l;\, \kappa,\, l')\ . \tag{4.2.3}$$

$G(n,\, l;\, \kappa,\, l')$ satisfy the recurrence relations

$$\begin{aligned} G(n,\, l;\, \kappa,\, l+1) \;=\; & -4n^2\left(n^2-(l+2)^2\right)\left[1+(l+3)^2\kappa^2\right]G(n,\, l+2;\, \kappa,\, l+3) \\ & +\left[4n^2-4(l+2)^2+(l+2)(2l+3)\left(1+n^2\kappa^2\right)\right]G(n,\, l+1;\, \kappa, l+2) \end{aligned}$$

$$\begin{aligned} G(n,\, l;\, \kappa,\, l-1) \;=\; & -4n^2\left[n^2-(l+2)^2\right]\left[1+(l+1)^2\kappa^2\right]G(n,\, l+2;\, \kappa,\, l+1) \\ & \left[4n^2-4(l+1)^2+(l+1)(2l+3)\left(1+n^2\kappa^2\right)G(n,\, l+1;\, \kappa,\, l)\right] \end{aligned}$$

with initial conditions

$$\begin{aligned} G(n,\, n-1;\, 0,\, n) &= \sqrt{\frac{\pi}{2}}\frac{1}{(2n-1)!}8n\,(4n)^n\,e^{-2n} \\ G(n,\, n-2;\, 0,\, n-1) &= \sqrt{\frac{\pi}{2}}\frac{1}{(2n-2)!}8n^2\,(4n)^n\,e^{-2n} \\ G(n,\, n-1;\, 0,\, n-2) &= \sqrt{\frac{\pi}{2}}\frac{1}{(2n-1)!}4\,(4n)^n\,e^{-2n} \\ G(n,\, n-2;\, 0,\, n-3) &= \sqrt{\frac{\pi}{2}}\frac{(n+3)}{(2n-2)!}4\,(4n)^n\,e^{-2n} \end{aligned}$$

if $\kappa = 0$ and

$$\begin{aligned}
G(n,\, n-1;\, \kappa,\, n) &= \sqrt{\frac{\pi}{2\left(1-\exp\left(-2\pi/\kappa\right)\right)}}\, 8n\,(4n)^n\, \frac{\exp\left[-2\kappa^{-1}\arctan\left(n\kappa\right)\right]}{(2n-1)!(1+n^2\kappa^2)^{n+2}} \\
G(n,\, n-2;\, \kappa,\, n-1) &= \sqrt{\frac{\pi}{2\left(1-\exp\left(-2\pi/\kappa\right)\right)}}\, 8n^2\,(4n)^n\, \frac{\exp\left[-2\kappa^{-1}\arctan\left(n\kappa\right)\right]}{(2n-2)!\left(1+n^2\kappa^2\right)^{n+1}} \\
G(n,\, n-1;\, \kappa,\, n-2) &= \sqrt{\frac{\pi}{2\left(1-\exp\left(-2\pi/\kappa\right)\right)}}\, 4\,(4n)^n\, \frac{\exp\left[-2\kappa^{-1}\arctan\left(n\kappa\right)\right]}{(2n-1)!(1+n^2\kappa^2)^{n+1}} \\
G(n,\, n-2;\, \kappa,\, n-3) &= \sqrt{\frac{\pi}{2\left(1-exp\left(-2\pi/\kappa\right)\right)}}\, \left(4+(n-1)\left(1+n^2\kappa^2\right)\right) 4\,(4n)^n \\
&\quad \times \frac{\exp\left[-2\kappa^{-1}\arctan\left(n\kappa\right)\right]}{(2n-2)!\left(1+n^2\kappa^2\right)^{n+1}}
\end{aligned}$$

otherwise.

$G(n,\, l;\, \kappa,\, l')$ is converted into $g(n,\, l;\, \kappa,\, l')$ by using two recurrence relations satisfied by the coefficients of (4.2.3). Let $g(n,\, l;\, \kappa\, l+1) = cu(l)G(n,\, l;\, \kappa\, l+1)$ and $g(n,\, l;\, \kappa\, l-1) = cl(l)G(n,\, l;\, \kappa\, l-1)$. Then the $cu\,(l)$ and $cl\,(l)$ satisfy

$$\begin{aligned}
cu(0) &= (2n)^{-n}\sqrt{\frac{n!}{(n-1)!}\left(1+\kappa^2\right)} \\
cu\,(l) &= cu(l-1)\, 2n\sqrt{\left(n^2-l^2\right)\left(1+(l+1)^2\,\kappa^2\right)}
\end{aligned}$$

and

$$\begin{aligned}
cl(1) &= (2n)^{1-n}\sqrt{\frac{(n+1)!}{(n-2)!}} \\
cl\,(l) &= cl(l-1)\, 2n\sqrt{\frac{(n+l)}{(n-l)}\left(1+(l-1)^2\,\kappa^2\right)}\,.
\end{aligned}$$

Burgess tabulates his results in terms of the quantity Θ given by

$$\Theta(n,\, l;\, \kappa,\, l') = z^2\left(1+n^2\kappa^2\right)\left|g(n,\, l;\, \kappa,\, l')\right|^2\,.$$

Because these recurrence relations do not involve division or square roots, working with $G(n,\, l;\, \kappa,\, l')$ instead of $g(n,\, l;\, \kappa,\, l')$ is more appropriate for fast computing. Burgess (1965) warns against severe scaling problems that may arise for large n

when calculating $G(n,\, l;\, \kappa,\, l')$ instead of $g(n,\, l;\, \kappa,\, l')$. This was overcome by doing calculations with the natural logarithm of $G(n,\, l;\, \kappa,\, l')$. The natural logarithm makes the number stored in the computer memory smaller, therefore avoiding overflow errors. To overcome the loss of precision of the numbers when using logarithms, all calculations were done in double precision. An additional advantage of working with logarithms is that multiplications are converted into additions and powers to multiplications, which speeds up calculations.

I implemented the method of Burgess (1965) to calculate the radial matrix element in a C program and the results from my code agreed with the values in the tables given by Burgess (1965), which are accurate to five significant figures.

4.2.2 Rate Coefficients

The radiative recombination coefficient was calculated using (2.2.2). Burgess (1965) gives an expression for the radiative recombination coefficient, using a Maxwellian distribution with a temperature T_e for the free electron velocities,

$$\alpha^r_{nl} = \left(\frac{2\pi^{1/2}\alpha^4 a_0^2 c}{3}\right)\frac{2y^{1/2}}{n^2} z \sum_{l'=l\pm1} I(n,\, l,\, l',\, T_e)$$

where

$$I(n,\, l,\, l',\, T_e) = \max(l,\, l') \int_0^\infty \left(1 + n^2\frac{y\kappa^2}{y}\right)^2 \Theta(n,\, l;\, \kappa,\, l')\, \mathrm{e}^{-y\kappa^2}\, d\big(y\kappa^2\big) \qquad (4.2.4)$$

and

$$y = \frac{z^2 Rhc}{kT_e}\,.$$

The form of the integral in (4.2.4) suggests the use of a Gauss-Laguerre quadrature scheme to integrate the equation numerically, but the accuracy of this integration scheme proved to be inadequate. The Gauss-Laguerre quadrature method does an n-point integration over the whole interval, but the derivative of the integrand is very large for small κ and decreases rapidly as κ increases.

Instead, a Gaussian integration method was used. This method does the integration over an arbitrary interval, so that smaller intervals can be used for small κ when

the integrand varies rapidly. A number of five-point Gaussian integrations are done starting with an interval size of $h = 10^{-4}n^{-1}$. The interval size was doubled after every five-point integration and the procedure was terminated when the sum of the integrals were accurate up to six significant digits.

The Gaussian integration scheme for an arbitrary interval is given by

$$\int_a^b f(y)\, dy \approx \frac{b-a}{2} \sum_{i=1}^{n} \omega_i f(y_i)$$

with

$$y_i = \left(\frac{b-a}{2}\right) x_i + \left(\frac{b+a}{2}\right) .$$

The abscissas x_i is given by the i^{th} zero of the Legendre polynomial $P_n(x)$, $P_n(1) = 1$. The weights ω_i are defined by

$$\omega_i = \frac{2}{1-x_i^2} \left[P_n'(x_i)\right]^2 .$$

Tables of x_i and ω_i are listed in Abramowitz & Stegun (1972).

The total radiative recombination rate coefficient to an energy level n is simply the sum of the coefficients resolved for the angular momentum states, so that

$$\alpha_n^r = \sum_{l=0}^{n-1} \alpha_{nl}^r .$$

Table 4.1 lists the total recombination coefficients to various energy levels for several electron temperatures.

Table 4.1 – Radiative recombination coefficients (in $\mathrm{cm^3\,s^{-1}}$) for hydrogen at various electron temperatures.

T_e	500 K	10 000 K	20 000 K	50 000 K
α_1^r	7.3457×10^{-13}	1.5815×10^{-13}	1.0784×10^{-13}	6.2108×10^{-14}
α_2^r	4.0046×10^{-13}	7.6946×10^{-14}	4.8421×10^{-14}	2.4049×10^{-14}
α_3^r	2.7283×10^{-13}	4.5524×10^{-14}	2.6684×10^{-14}	1.1948×10^{-14}
α_{10}^r	7.1260×10^{-14}	2.4633×10^{-15}	2.5862×10^{-15}	9.0087×10^{-16}
α_{50}^r	4.2917×10^{-15}	1.2050×10^{-16}	4.9215×10^{-17}	1.4712×10^{-17}
α_{100}^r	8.8224×10^{-16}	1.9583×10^{-17}	7.7629×10^{-18}	2.2489×10^{-18}
α_{200}^r	1.5824×10^{-16}	3.0162×10^{-18}	1.1718×10^{-18}	3.3217×10^{-19}

The photoionization cross-section to level nl for a hydrogenic atom or ion was calculated using the formula of Burgess & Seaton (1960)

$$a_{nl}^p\big(k^2\big) = \left(\frac{4\pi\alpha a_0^2}{3}\right)\frac{n^2}{z^2}\sum_{l'=l\pm1}\frac{\max\left(l,\,l'\right)}{2l+1}\Theta(n,\,l;\,\kappa,\,l')\ . \tag{4.2.5}$$

Putting (4.2.5) into (2.2.3) and using (4.2.1), the photoionization coefficient α_{nl} can be written as

$$\alpha_{nl}^p = \left(\frac{4\pi R c\alpha a_0^2}{3}\right)\frac{n^2}{2l+1}\int_0^\infty\left(\frac{4\pi J_\nu}{h\nu}\right)_{\kappa^2}\sum_{l'=l\pm1}\max\left(l,\,l'\right)\Theta(n,\,l;\,\kappa,\,l')\ d\left(\kappa^2\right) \tag{4.2.6}$$

where χ_{nl} is the ionization energy of the level nl. The subscript κ^2 indicates that the quantity inside the brackets should be written in terms of κ^2 before integration.

The integral in (4.2.6) was handled in the same manner as for radiative recombination.

The total photoionization coefficient for hydrogen from level n is given by

$$\alpha_n^p = \sum_{l=0}^{n-1}\frac{2l+1}{n^2}\alpha_{nl}^p\,.$$

Photoionization coefficients for blackbody radiation fields at various temperatures are shown in Table 4.2.

Table 4.2 – Photoionization coefficients α_n^p (in $\mathrm{cm^3\,s^{-1}}$) where n is the principal quantum number of hydrogen in a ionized plasma permeated by an external radiation field with an undiluted blackbody spectrum defined by temperatures T_r.

T_r	100 K	20 000 K	40 000 K
c	—	2.7562×10^{5}	2.6981×10^{7}
α_2^p	—	1.2488×10^{7}	6.7718×10^{7}
α_3^p	1.1887×10^{-71}	1.1494×10^{7}	3.7567×10^{7}
α_{10}^p	6.3523×10^{-4}	8.4442×10^{5}	1.8156×10^{6}
α_{50}^p	1.6815×10^{1}	7.9020×10^{3}	1.5886×10^{4}
α_{100}^p	3.7476×10^{0}	9.9487×10^{2}	1.9929×10^{3}
α_{200}^p	5.6767×10^{-1}	1.2458×10^{2}	2.4927×10^{2}

Milne (1924) extended the Einstein relations between the bound-bound rate coefficients to the bound-free case. The resulting equations are known as the Einstein-Milne equations and give relationships between the radiative bound-free cross-sections. The stimulated recombination cross-section is related to the photoionization cross-section by

$$\sigma_{nl}^s = \frac{g_{nl}}{8\pi g_i} \frac{h^2}{m_e^2 v^2} a_{nl}^p \,. \tag{4.2.7}$$

The degeneracy of level nl of a hydrogenic ion or atom is $g_{nl} = 2\,(2l+1)$.

Putting (4.2.5) into (4.2.7) to find the stimulated recombination cross-section, and in turn putting the result into (2.2.4) gives the stimulated recombination coefficient as

$$\begin{aligned} \alpha_{nl}^s \;=\; & \left(\frac{4\pi R c \alpha a_0^2}{3}\right) \left(\frac{m}{2\pi k T}\right)^{3/2} \left(\frac{h}{m}\right)^3 n^2 \\ & \times \int_0^\infty \left(\frac{4\pi J_\nu}{h\nu}\right)_{\kappa^2} \sum_{l'=l\pm1} \max(l,\, l')\, \Theta(n,\, l;\, \kappa,\, l')\, e^{-y\kappa^2} d(\kappa^2) \end{aligned}$$

The integration was handled using a Gaussian quadrature scheme as described above for radiative recombination.

The total stimulated recombination coefficient to an energy level n of hydrogen is

given by

$$\alpha_n^s = \sum_{l=0}^{n-1} \alpha_{nl}^s \,.$$

Total stimulated recombination rate coefficients for a plasma at electron temperatures permeated by a blackbody radiation field are listed in Table 4.3. Note that the radiation fields are undiluted and therefore not necessarily representative of astronomical environments.

Table 4.3 – Stimulated recombination coefficients α_n^s (in $\mathrm{cm^3\,s^{-1}}$) for hydrogen in a plasma with electron temperature T_e and permeated by a radiation field with an undiluted blackbody spectrum with a temperature T_r.

T_r	100 K		40 000 K	
T_e	5 000 K	10 000 K	10 000 K	20 000 K
α_1^s	—	—	2.5057×10^{-15}	1.4448×10^{-15}
α_2^s	—	—	3.4380×10^{-14}	1.8445×10^{-14}
α_3^s	1.2287×10^{-91}	4.3870×10^{-92}	5.7034×10^{-14}	2.7978×10^{-14}
α_{10}^s	7.3021×10^{-23}	2.6060×10^{-23}	5.7682×10^{-14}	2.2736×10^{-14}
α_{50}^s	4.8752×10^{-17}	1.7322×10^{-17}	1.6004×10^{-14}	5.7283×10^{-15}
α_{100}^s	4.3682×10^{-17}	1.5482×10^{-17}	8.1797×10^{-15}	2.9038×10^{-15}
α_{200}^s	2.6543×10^{-17}	9.3940×10^{-18}	4.1177×10^{-15}	1.4577×10^{-15}

4.2.3 Verification of Coefficients

The values of the bound-free coefficients were checked by comparing them to values generated using the method described in Burgess & Summers (1976). They do not give values explicitly, so their method had to be coded to allow for comparison of values. The values generally agreed to at least four significant digits, with the largest deviation occurring for small values of n. Because Burgess & Summers (1976) used an approximation for the bound-free Gaunt factor, this is understandable.

Another control was done by only including the radiative bound-free processes in (3.1.4) and ignoring all other processes. By the principle of detailed balance, all the departure coefficients should be equal to unity if the whole system is in thermal

equilibrium, that is $T_e = T_r$, where T_r is a temperature describing a blackbody spectrum. This gave $b_n = 1$ for all n and all temperatures $T_e = T_r$.

4.3 Collisional Transitions

The semi-empirical formulae of Vriens & Smeets (1980) were used to calculate the collisional excitation rate coefficients for collisional bound-bound transitions. Because the values are valid over a wider range of temperature, these were used in favour of the more commonly used formulae of Gee et al. (1976). Vriens & Smeets (1980) claim that their values agree within 5 to 20 % with those of Gee et al. (1976). Collisional cross-sections involve three-body processes and hence can only be determined using approximations in the calculations. The calculational uncertainties are of the order of 20 %.

The excitation rate coefficient is given in $\mathrm{cm}^3\,\mathrm{s}^{-1}$ by

$$C_{n'n} = \frac{1.6 \times 10^{-7}\sqrt{kT_e}}{kT_e + \Gamma_{n'n}} \exp\left(\frac{-E_{n'n}}{kT_e}\right) \times \left[a_{n'n} \ln\left(\frac{0.3kT_e}{R} + \Delta_{n'n}\right) + b_{n'n}\right] \quad (4.3.1)$$

with

$$\begin{aligned}
\Delta_{n'n} &= \exp\left(-\frac{b_{n'n}}{a_{n'n}}\right) + \frac{0.06s^2}{n\left(n'\right)^2}\,, \\
\Gamma_{n'n} &= R\ln\left(1 + \frac{\left(n'\right)^3 kT_e}{R}\right)\left[3 + 11\left(\frac{s}{n'}\right)^2\right] \\
&\qquad \times \left(6 + 1.6ns + \frac{0.3}{s^2} + 0.8\frac{n^{1.5}}{\sqrt{s}}\left|s - 0.6\right|\right)^{-1}\,, \\
a_{n'n} &= \frac{2Rf_{n'n}}{E_{n'n}}\,, \\
f_{n'n} &= \left(\frac{n'}{n}\right)^2 \frac{mc^3}{8\pi^2 e^2 \nu_{nn'}^2} \\
b_{n'n} &= \frac{4R^2}{n^3}\left(\frac{1}{E_{n'n}} + \frac{4E_{n'i}}{3E_{n'n}^3} + t_{n'}\frac{E_{n'i}^2}{E_{n'n}^4}\right)\,, \\
t_{n'} &= \frac{1.4\ln\left(n'\right)}{n'} - \frac{0.7}{n'} - \frac{0.51}{\left(n'\right)^2} + \frac{1.16}{\left(n'\right)^3} - \frac{0.55}{\left(n'\right)^4}\,, \\
s &= \left|n - n'\right|
\end{aligned}$$

where R is the Rydberg energy, e is the elementary charge, $E_{n'i}$ is the ionization energy of level n' and $f_{n'n}$ is the absorption oscillator strength. The frequency $\nu_{nn'}$ is the frequency associated with the transition given by (4.1.2). Fig. 4.1 shows the temperature dependence of the excitation rate coefficient as given by (4.3.1) for various transitions.

The de-excitation rate coefficients were calculated using (2.3.2). Vriens & Smeets (1980) claim that their values agree within 5 to 20% with experiment.

The rates of bound-free collisional processes were also calculated using the formulae given by Vriens & Smeets (1980). The collisional ionization coefficient is given by

$$C_{ni} = \frac{9.56 \times 10^{-6} \left(kT_e\right)^{-1.5} \exp\left(-\epsilon_{ni}\right)}{\epsilon_{ni}^{2.33} + 4.38\epsilon_{ni}^{1.72} + 1.32\epsilon_{ni}} \tag{4.3.2}$$

where $\epsilon_{ni} = E_{ni}/kT_e$. Using the Saha-Boltzmann equation, the three-body recombination coefficient is given by

$$C_{in} = \frac{3.17 \times 10^{-27} \left(kT_e\right)^{-3} \left(g_n/g_i\right)}{\epsilon_{ni}^{2.33} + 4.38\epsilon_{ni}^{1.72} + 1.32\epsilon_{ni}} \,,$$

where g_n and g_i are the statistical weights of level n and the ion ground state respectively. C_{in} has units of $\mathrm{cm}^6\,\mathrm{s}^{-1}$. Vriens & Smeets (1980) found that their formulae agreed within 10 to 30 % with experimental data. Rate coefficients as a function of electron temperature as given by (4.3.2) are shown in Fig. 4.2.

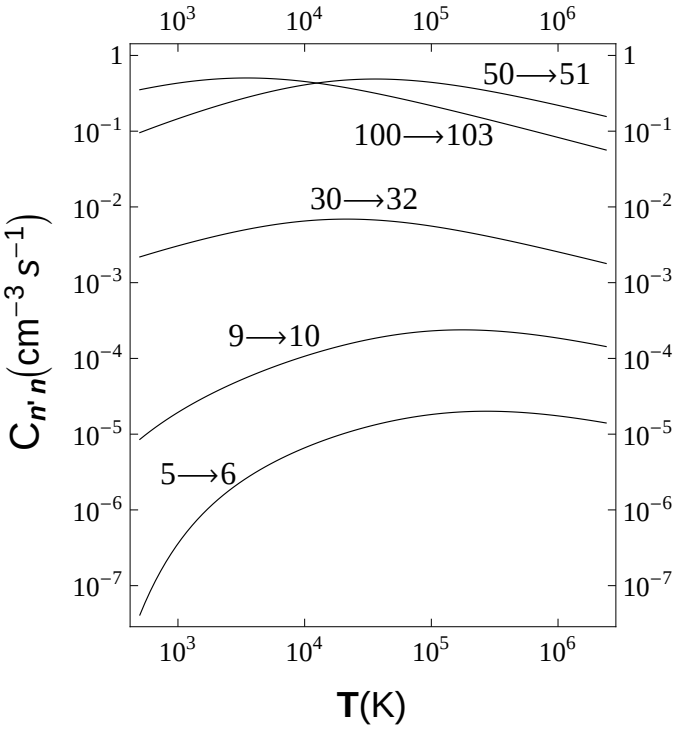

Figure 4.1 – Rate coefficients for excitation by electron impact for some bound-bound transitions of hydrogen calculated using the method of Vriens & Smeets (1980).

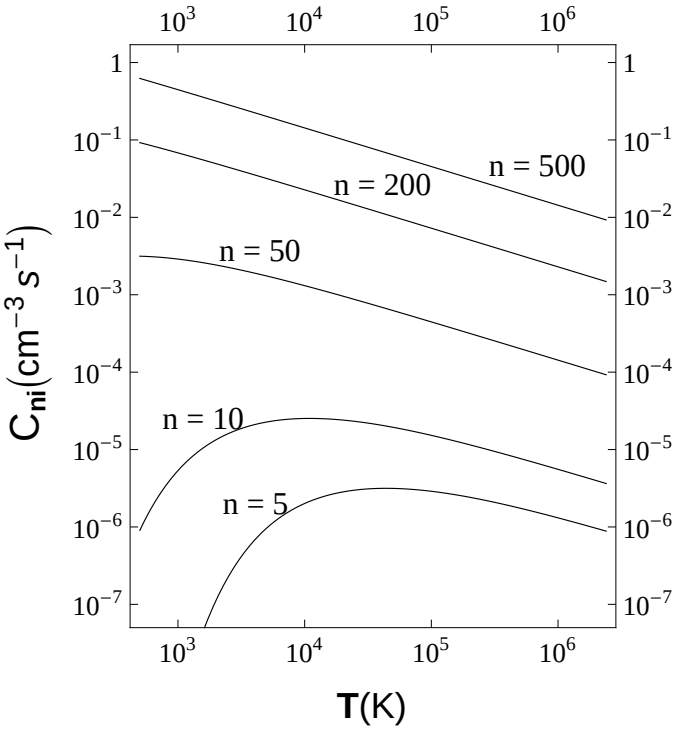

Figure 4.2 – Collisional ionization rate coefficients due to electron impact in a plasma to various energy levels of hydrogen.

4.3.1 Verification of Coefficients

As an additional check on the collisional coefficients, all non-collisional processes were set to zero in the rate equation (3.1.4) and departure coefficients were calculated using the developed codes. This resulted in all of the departure coefficients coming out equal to unity, as is expected by the principle of detailed balance.

Chapter 5

Numerical Methods

A model such as the one described here does calculations of atomic rates using quantum mechanical expressions and can be very computationally intensive and take a long time to run. Due to the technological advancement of computers, this is much less problematic today than it was when some of the previous models were developed. Nevertheless, it is still necessary to employ numerical methods to keep the run time reasonable and not exhaust the dynamic memory of the computer. This chapter describes the numerical methods that have been employed to keep the execution of the program practical, without compromising too much on the accuracy of the results.

5.1 Transition Rates Close to the Ionization Limit

In principle, an atom has an infinite number of energy levels and thus the solution of the population structure of hydrogen requires the solution of an infinite number of coupled equations as discussed in § 3.1. To make the mathematics computationally viable, I introduced an upper cut-off n_{max} for the highest n level for which the rate equation (3.1.5) were solved explicitly. The influence of levels above n_{max} are still taken into account, but they are handled in a different way to levels below n_{max}. Departure coefficients are only calculated for levels up to n_{max}; levels above the cut-off will be discussed presently.

It was found that the departure coefficients above $n = 500$ are always equal to unity for nebular conditions, so there is no need to calculate the departure coefficients

explicitly for levels above $n = 500$. The cut-off, n_{max}, is set to 496; the significance of this number will be discussed in § 5.2. Equation (3.1.5) is then altered to

$$\begin{aligned}
&\left(\frac{2\pi m_e k_B T}{h^2}\right)^{3/2} (\alpha_n^r + \alpha_n^s + N_e C_{i,n}) - n^2 e^{\chi_n/k_B T} \sum_{m=497}^{\infty} (N_e C_{nm} + B_{nm} J_\nu) \\
&\qquad + \sum_{m=497}^{\infty} m^2 e^{\chi_m/k_B T} (A_{mn} + N_e C_{mn} + B_{mn} J_\nu) \\
= \; & b_n n^2 e^{\chi_n/k_B T} \left[\alpha_n^p + N_e C_{n,i} + \sum_{k<n} (A_{nk} + N_e C_{nk} + B_{nk} J_\nu) \right. \\
&\qquad \left. + \sum_{m>n}^{496} (N_e C_{nm} + B_{nm} J_\nu) \right] - \sum_{k<n} b_k k^2 e^{\chi_k/k_B T} (N_e C_{kn} + B_{kn} J_\nu) \\
&\qquad - \sum_{m>n}^{496} b_m m^2 e^{\chi_m/k_B T} (A_{mn} + N_e C_{mn} + B_{mn} J_\nu) \; .
\end{aligned} \tag{5.1.1}$$

The consequence of this on the matrix scheme presented in § 3.1 is that the components of the row vector $\mathbf{a}$ defined in (3.1.6) become

$$\begin{aligned}
\mathrm{a}_n \; = \; & \left(\frac{2\pi m_e k_B T}{h^2}\right)^{3/2} (\alpha_n^r + \alpha_n^s + N_e C_{i,n}) - n^2 e^{\chi_n/k_B T} \sum_{m=497}^{\infty} (N_e C_{nm} + B_{nm} J_\nu) \\
&\qquad + \sum_{m=497}^{\infty} m^2 e^{\chi_m/k_B T} (A_{mn} + N_e C_{mn} + B_{mn} J_\nu) \; .
\end{aligned} \tag{5.1.2}$$

The elements of the matrix $\mathbf{X}$ remain unchanged, taking into account that all sums over m go up to 496.

The sums to infinity in (5.1.2) were handled as follows. Firstly, the sum was converted to an integral using the trapezoidal rule, so that

$$\begin{aligned}
&\sum_{m=497}^{\infty} \left[m^2 e^{\chi_m/k_B T} (A_{mn} + N_e C_{mn} + B_{mn} J_\nu) - n^2 e^{\chi_n/k_B T} (N_e C_{nm} + B_{nm} J_\nu) \right] \\
\approx \; & \int_{497}^{\infty} m^2 e^{\chi_m/k_B T} (A_{mn} + N_e C_{mn} + B_{mn} J_\nu) - n^2 e^{\chi_n/k_B T} (N_e C_{nm} + B_{nm} J_\nu) \, dm \, .
\end{aligned}$$

This integral was then approximated using a 20-point Gaussian quadrature which works as follows. An integral over an arbitrary interval (a, b) can be approximated as

$$\int_a^b f(y)\, dy \approx \frac{b-a}{2} \sum_{i=1}^{n} \omega_i f(y_i)$$

where

$$y_i = \left(\frac{b-a}{2}\right) x_i + \left(\frac{b+a}{2}\right) .$$

The y_i are in general not integers and the rate coefficients in the numerical integration scheme were calculated for the two integers nearest to y_i. This resulted in two values for $f(y_i)$ for every iteration and the result of a linear interpolation of the two values was finally used.

There are physical limits to the number of energy levels that an atom can have in a gas that need to be considered to determine the upper bound of the integration b to represent the ionization limit. An electron cannot be bound if it is further than the Debye length

$$\lambda_D = \sqrt{\frac{kT_e}{4\pi e^2 N_e}}$$

from the nucleus, since a sphere with radius λ_D represents the volume of influence of the nucleus. Because the free electrons in the plasma will screen charge of the nucleus, an electron further away than λ_D from the nucleus cannot be bound to the nucleus.

Also, an electron cannot be considered to be bound by a nucleus if it exists in the electron cloud of another nucleus. The radius of the average spherical volume occupied per particle is given by the Wigner–Seitz radius

$$r_s = \left(\frac{3}{4\pi N_e}\right)^{1/3} .$$

According to the Bohr theory, the radius of a hydrogenic atom with a valence electron in the nth energy level is given by

$$r_n = \frac{a_0 n^2}{Z} .$$

Therefore, the condition

$$b < n_c = \sqrt{\frac{Z\ \min(\lambda_D,\, r_s)}{a_0}}$$

must always hold.

It was found that n_c ranges from 1 082 to 5 025 for

$$T_e/\mathrm{K},\ N_e/\mathrm{cm}^{-3} \in \left(10^2,\ 10^6\right)\ ,$$

which are the ranges relevant to many interstellar plasmas. The upper limit was taken to be $b = 1\,000$ as transitions to and from energy levels beyond this limit contribute negligibly to the populations of levels with $n < 496$.

5.2 Matrix Condensation

Burgess & Summers (1969) introduced a matrix condensation technique based on Lagrange interpolation which has been used by a number of authors. The technique condenses the sizable matrix $\mathbf{X}$ described in § 3.1 to a much smaller matrix, which can be readily inverted. From a computational point of view, it is necessary to condense the matrix to economize the dynamic memory used by the computer. Because the matrix has to be inverted, two matrices of equal size have to be used and without condensation this results in two 496×496 matrices that have to be stored in the memory at one time. Because the departure coefficients vary smoothly and slowly with n, the condensation technique can be applied. The method is presented in more detail here than the rather terse explanation giving by Burgess & Summers (1969).

For each n we are required to solve the system of equations

$$a(n) = \sum_{i=n_0}^{n_{max}} b(i)X(i,\ n) \tag{5.2.1}$$

where $n_0 = 1$ for Case A and $n_0 = 2$ for Case B of Baker & Menzel (1938). The distinction between the two cases will be described more fully in Chapter 7.

A selected set of sublevels is represented by the the array $m(t)$ so that $t = 1,\ 2,\ \ldots,\ M$ where $M < n_{max}$ and

$$m(1) = 1, \qquad m(t) < m(t+1), \qquad m(M) = n_{max}\,.$$

Let $\bar{\mathbf{a}}$ and $\bar{\mathbf{b}}$ represent condensed arrays so that

$$\bar{a}(t) = a(m(t)) \qquad \text{and} \qquad \bar{b}(t) = b(m(t))\,.$$

We can obtain $\mathbf{b}$ from $\bar{\mathbf{b}}$ using the Lagrangian interpolation formula

$$b\,(i) = \sum_{t=1}^{M} \bar{b}\,(t)\,L\,(t,\,i) \tag{5.2.2}$$

where the interpolation weights are given by

$$L\,(t,\,i) = 0 \qquad \text{if } \; t < t_1 \text{ or } t > t_2$$

and

$$L\,(t,\,i) = \prod_{\substack{\tau=t_1 \\ \tau \neq t}}^{t_2} \frac{m\,(\tau) - i}{m\,(\tau) - m\,(t)} \qquad \text{if } t_1 \leq t \leq t_2\,.$$

In general, t_1 and t_2 will depend on i. For any two adjacent sublevels $m(x-1)$ and $m(x)$, values of $i \,\forall\, m(x-1) \leq i \leq m(x)$ will be interpolated using a polynomial of order $h = h\,(x) = m\,(x) - m(x-1)$. For every interval $m(x) - h/2 \leq i \leq m(x) + h/2$, we will have $t_1 = x - h/2$ and $t_2 = x + h/2$. Care has to be taken when x is small or approaches M, as we must always have $t_1 \geq 1$ and $t_2 \leq M$.

Letting $n = m\,(s)$ and substituting (5.2.2) into (5.2.1) gives

$$a\,(m\,(s)) = \sum_{t=1}^{M} \bar{b}\,(t) \sum_{i=n_0}^{n_{max}} L\,(t,\,i)\,X(i,\,m\,(s))\,.$$

Thus we can write

$$\bar{a}\,(s) = \sum_{t=1}^{M} \bar{b}\,(t)\,\bar{X}\,(t,\,s)$$

where

$$\bar{X}\,(t,\,s) = \sum_{i=n_0}^{n_{max}} L\,(t,\,i)\,X(i,\,m\,(s))\,.$$

The method condenses the $n_{max} \times n_{max}$ matrix $\mathbf{X}$ to an $M \times M$ matrix $\bar{\mathbf{X}}$. We can calculate $\bar{\mathbf{b}}$ using

$$\bar{\mathbf{b}} = \bar{\mathbf{a}} \cdot \bar{\mathbf{X}}^{-1}$$

and interpolate $\bar{\mathbf{b}}$ to the full set of departure coefficients $\mathbf{b}$ using (5.2.2).

The departure coefficients vary the fastest as a function of n for small n, so it is suitable to choose $h(x)$ small for small n, increasing in magnitude as n increases and the departure coefficients vary more slowly. The subset $m(t)$ was chosen such that $M = 100$ and $h(t) = 1$ for $t \in [1, 20]$ (no interpolation used). The h was then increased in step sizes of 2, up to 9, for every 20 iterations.

At the transition points when $h(x) \neq h(x+1)$ it is necessary to enforce an additional condition. For such points $h(x+1) = h(x+2) - 1$ to ensure that the point $m(x)+1$ can be interpolated. For example, $\{h(20), h(21), h(22), h(23)\} = \{1, 2, 3, 3\}$, so that the subset is given by $\{m(19), m(20), m(21), m(22), m(23)\} = \{19, 20, 22, 25, 28\}$. Applying this procedure leads to $m(M) = 496$, which is the reason n_{max} was set to 496 in § 5.2.

Chapter 6

Hydrogen Population Structure

The results for the hydrogen population structure, under various conditions, are presented here using the developed codes. The departure coefficients were calculated using codes developed based on the theory and techniques developed in the preceding chapters. Results for capture-cascade and capture-collision-cascade (C^3) models are presented and compared to corresponding existing models. Results for C^3 models permeated by a radiation field are also given.

6.1 Capture-Cascade Model

Capture-cascade models are the simplest models for recombination nebulae. In these models, ions and electrons recombine only by radiative recombination, and bound electrons cascade downwards to lower energy levels through spontaneous emissions. Collisional effects and the ionizing radiation field are disregarded.

Capture-cascade models are a good approximation for low energy levels when the electron density is small and become exact as $N_e \to 0$. Low electron densities ensure that collisions occur infrequently and the collisional processes are not important in determining the departure coefficients. Radiative recombination and spontaneous emissions are the dominant processes for low energy levels, so that departure coefficients tend towards the results of a capture-cascade model when the principal quantum number n is small.

Descriptions of capture-cascade models can be found in Burgess (1958), Seaton (1959) and Pengelly (1964). Notably, Seaton (1959) presented a capture-cascade

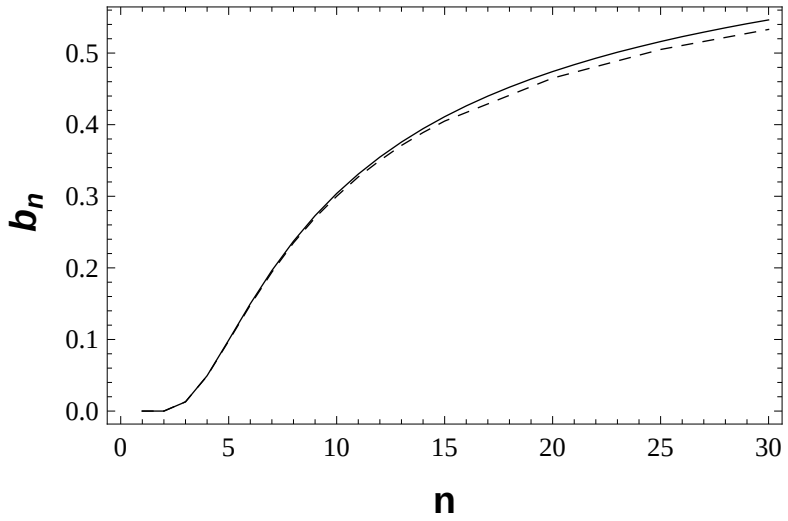

Figure 6.1 – Comparison between the results of Seaton (1959) (dashed line) and the departure coefficients presented in this work (solid line) for a capture-cascade model. Results shown are for a hydrogen nebula with a temperature of $T_e = 5\,000\,\mathrm{K}$, assuming Case B.

model using a cascade matrix technique, which is similar, in essence, to the matrix technique presented here. A comparison between the results of Seaton (1959) and this work (with $N_e = 0$) is shown in Fig. 6.1.

The departure coefficients calculated in this work and the results given in Seaton (1959) agree on average within 0.2 %, with the results diverging as n increases. The deviations are expected, since the transition rates that were used are different, with the rates of Seaton (1959) being more approximate. The way in which the contributions of levels up to the ionization limit were calculated is also different.

6.2 Capture-Collision-Cascade Model

A C^3 model takes collisional processes induced by free particles into account, in addition to the pure radiative processes considered in a capture-cascade model. Because collisional processes become more important than radiative processes in determining the level populations for large n, the inclusion of collisional processes is a very important step to extend results to higher energy levels, .

Fig. 6.2 illustrates how the rates of collisional processes become much larger than radiative processes for large enough principal quantum number. The left panel

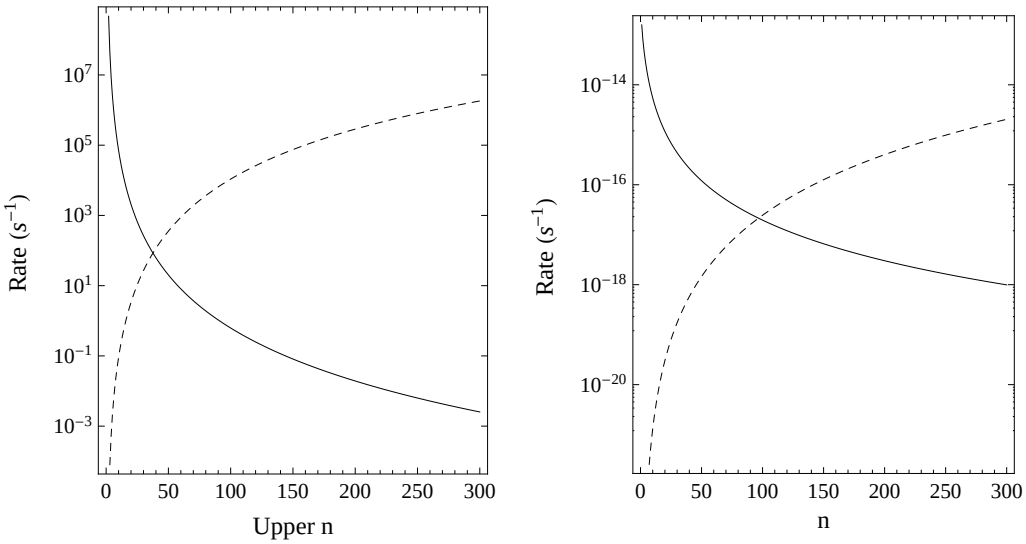

Figure 6.2 – Comparison of radiative and collisional transitions rates at various energy levels. The left panel shows bound-bound radiative rates $A_{n,n-1}$ (solid line) with the collisional rates $N_e C_{n,n-1}$ (dashed line) for the same transition for a plasma with electron density $N_e = 10^3\,\mathrm{cm}^{-3}$ and electron temperature $T_e = 10^4\,\mathrm{K}$. The right panel shows a comparison between the rates of radiative recombination α_n^r (solid line) and three-body recombination $N_e C_{in}$(dashed line) for the same plasma.

shows the rate of collisional de-excitation compared to that of spontaneous emission for transitions of the type $n \to n-1$, and the right panel shows a comparison of the rates of radiative and three-body recombination. From the graphs it is clear that radiative processes dominate at low energy levels when the radiative rates are much faster than the collisional rates, which is why capture-cascade models give good results for these levels. Collisional processes become more important as the principal quantum number increases and dominate over radiative processes for high energy levels.

The collisional processes and their inverses are related by the Boltzmann equation for bound-bound processes, or the Saha-Boltzmann equation for bound-free processes. This means that if only the collisional processes are present, all departure coefficients would be equal to unity as the collisional processes set up a Boltzmann distribution.

Fig. 6.3 shows the effect of the electron density on the population structure of a hydrogen plasma at temperature $T_e = 10^4\,\mathrm{K}$. The dashed line represents the radiative limit where collisional processes are disregarded. As the collisional processes start to dominate for increasing n, the departure coefficients deviate from the radiative limit

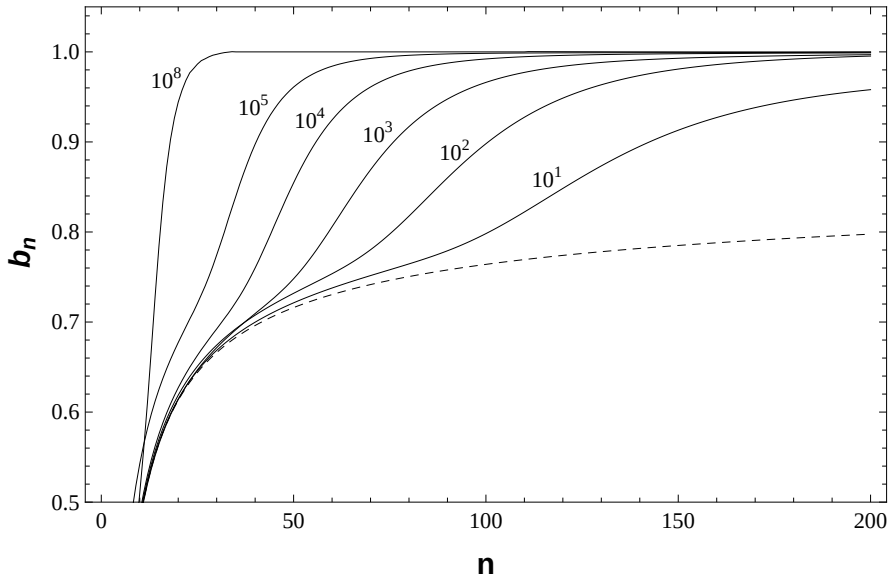

Figure 6.3 – Population structure of hydrogen for a plasma at $T_e = 10^4\,\mathrm{K}$ with various electron densities. The dashed line represents the radiative limit ($N_e = 0\,\mathrm{cm}^{-3}$) as calculated with a capture-cascade model.

and are forced towards the collisional limit where $b_n = 1\,\forall\, n$. The transition from the radiative to the collisional dominated regions occurs at lower n as N_e increases.

From Fig. 6.3 it can be seen that the departure coefficients always appear to be less than or equal to one, i.e. the level populations are lower than or equal to what is expected in TE. Spontaneous emission, which dominates at low n levels, has no inverse process to balance it and it empties the atomic levels very rapidly. The ground state ($n = 1$) cannot be emptied via spontaneous emissions and is mainly emptied by photoionizations. The rate of photoionizations from the ground state is much slower than that of spontaneous emissions into the ground state and it becomes overpopulated with $b_1 \gg 1$. This is also the case for the $n = 2$ level under the assumption of Case B (see § 7.1 for a discussion on Case A and B). Higher levels can also become overpopulated under certain extreme conditions, such as when the gas is exposed to a very intense radiation field.

Descriptions of C^3 models can be found in Brocklehurst (1970), Hummer & Storey (1987) and Smits (1991). The results of this work for an n-method C^3 model agree on average within 0.5 % with the results of Brocklehurst (1970) and 0.3 % with that of Smits (1991). The tables of Hummer & Storey (1987) are not comparable to this work for low n-levels, as their results are for an nl-model. For $n \geq 70$ the results of this word agree on average within 0.4 % with their tables.

6.3 Capture-Collision-Cascade Model with a Radiation Field

An important step in plasma modelling is to include the effects of the ionizing radiation field on the population structure of the atoms in the gas. Recombination plasmas, which are the focus of this work, are permeated by an external radiation field that ionizes a larger fraction of the atoms. We can then observe spectral lines that result from electrons recombining with nuclei. The radiation field has to be relatively strong, for if it were too weak to ionize the gas a recombination spectrum will not be observed.

In general it is important to take the ionizing radiation into account, but this cannot be described by recombination theory alone and it is necessary to do radiative transfer calculations. The radiation changes as it propagates through the gas and the gas itself will absorb photons at specific frequencies as well as emit a diffuse radiation field. The b_n problem will then depend on many more parameters than for a C^3 model, in particular it will be geometry-dependent.

If the source of ionizing radiation is behind the nebula that is being observed, observed lines will be amplified by stimulated emission.If the ionizing source is in front of the nebula, the departure coefficients will still depend on the radiation field, but observed lines will not be amplified by stimulated processes. The level populations will be affected regardless of where the ionizing source is. In this work, the effects of a radiation field on the departure coefficients is investigated, but the amplification of lines will not be considered.

6.3.1 Diluted Blackbody Radiation

The source of the ionizing radiation field is usually a star or a group of stars, so the ionizing spectrum can be approximated by a blackbody spectrum, or the superposition of blackbody spectra. The mean intensity of the external radiation field is represented by

$$J_\nu \, d\nu = \frac{2h\nu^3}{c^2} \frac{W \, d\nu}{e^{h\nu/kT_r} - 1}$$

where T_r is the temperature of the radiation. The parameter W is a dilution factor that is introduced based on geometrical considerations of the system. For a single

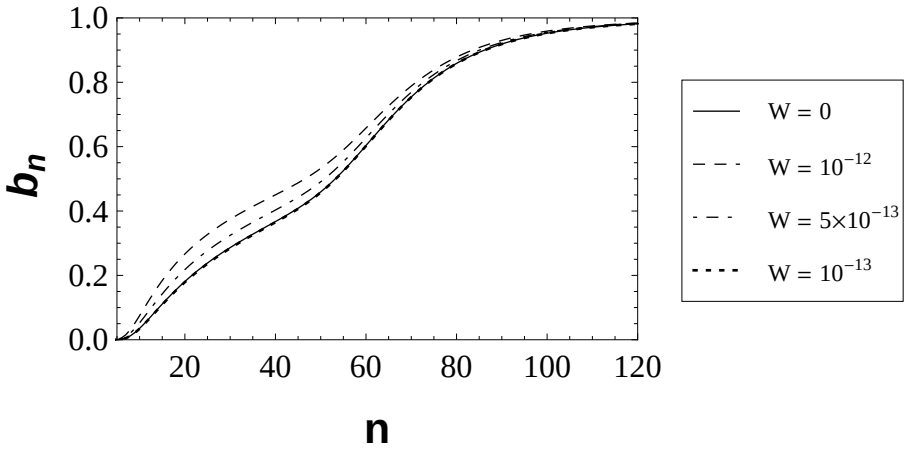

Figure 6.4 – Effect on the population structure of hydrogen of a diluted blackbody radiation field with temperature $T_r = 40\,000\,\mathrm{K}$ with various dilution factors. Parameters for the nebula was taken as $T_e = 10^3\,\mathrm{K}$ with $N_e = 10^3\,\mathrm{cm}^{-3}$, assuming Case B. The solid line shows the population structure if no radiation field is present.

ionizing star with a radius of R, the dilution factor at a distance d from the star will be

$$W \approx \frac{1}{4}\left(\frac{R}{d}\right)^2 \quad \text{for} \quad d \gg R\,.$$

For an O star with $R = 18R_\odot$, the dilution factor is $W \sim 10^{-16}$ at a distance of 10 pc and $W \sim 10^{-14}$ at 1 pc.

Fig. 6.4 shows the effect that a diluted blackbody field has on the population structure of hydrogen for a plasma with $T_e = 10^3\,\mathrm{K}$ and $N_e = 10^3\,\mathrm{cm}^{-3}$. The radiation temperature was taken as $T_r = 40\,000\,\mathrm{K}$ to represent an O star. For a relatively dense radiation field ($W = 10^{-12}$, 5×10^{-13}), the departure coefficients are larger than they are if no radiation field is present. For less dense fields, the departure coefficients are lowered by the radiation field, as can be seen for the case $W = 10^{-13}$ in Fig. 6.4. As the density of the field decreases, the b_n values approach the $W = 0$ case asymptotically from below.

Fig. 6.5 is similar to Fig. 6.2, but compares rates of processes stimulated by a radiation field as well. Rates are shown for the conditions described in Fig. 6.4 for $W = 10^{-12}$. From the graph it can be seen why the effects of the radiation field are most pronounced for $15 < n < 60$. In this region, the combined rates of the spontaneous and collisional transitions are the smallest, allowing stimulated effects to become more pronounced than for other values of n. Note that the plots are shown on a logarithmic scale.

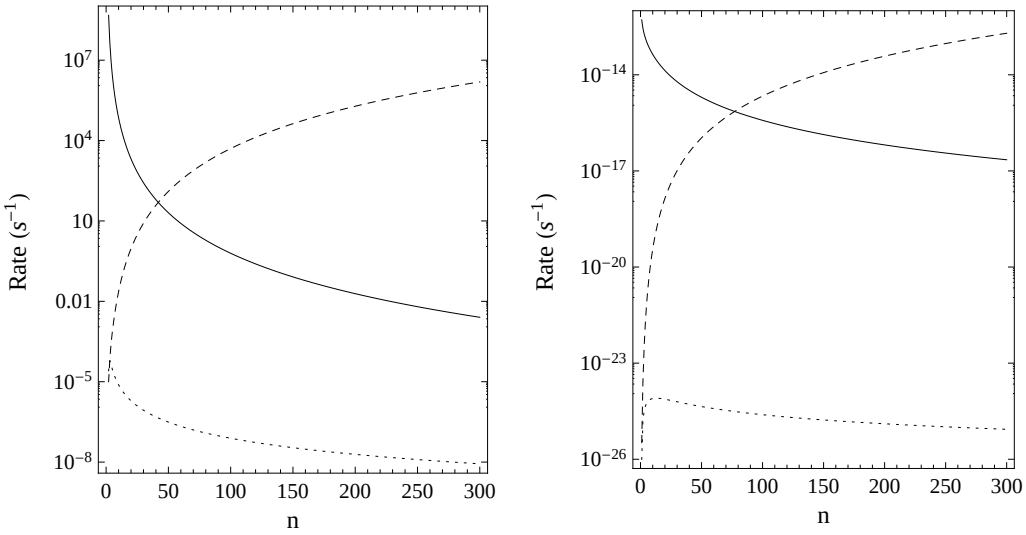

Figure 6.5 – Comparison of spontaneous radiative, collisional and stimulated transitions rates at various energy levels. The left panel shows bound-bound radiative rates $A_{n,n-1}$ (solid line), the collisional rates $N_e C_{n,n-1}$ (dashed line) and the stimulated emission rate $B_{n,n-1}J_\nu$ (dotted line) for the same transition for a plasma described in Fig. 6.4 with $W = 10^{-12}$. The right panel shows a comparison between the rates of radiative recombination α_n^r (solid line), three-body recombination $N_e C_{in}$(dashed line) and stimulated recombination α_n^s (dotted line) for the same plasma.

The effect of the stimulated processes increases as the electron density decreases, which means the collisional processes are less important. The effect increases significantly as the temperature of the radiation increases, as expected.

6.3.2 Cosmic Microwave Background Radiation

Even though the cosmic microwave background radiation (CMBR) has a blackbody spectrum of only 3 K, it is very dense and hence affects the population structure of hydrogen atoms. The result of a 3 K blackbody radiation field on the population structure of hydrogen was examined for 16 environments with parameters $10\,\mathrm{cm}^{-3} < N_e < 10^4\,\mathrm{cm}^{-3}$ and $300\,\mathrm{K} < T_e < 20\,000\,\mathrm{K}$. The effects is most noticeable in cool clouds with low electron densities. The 3 K blackbody radiation field affects the population structures most typically for $50 < n < 150$, increasing the departure coefficients slightly for these levels. The departure coefficients for higher levels are less affected and can increase or decrease, depending on the exact conditions. In

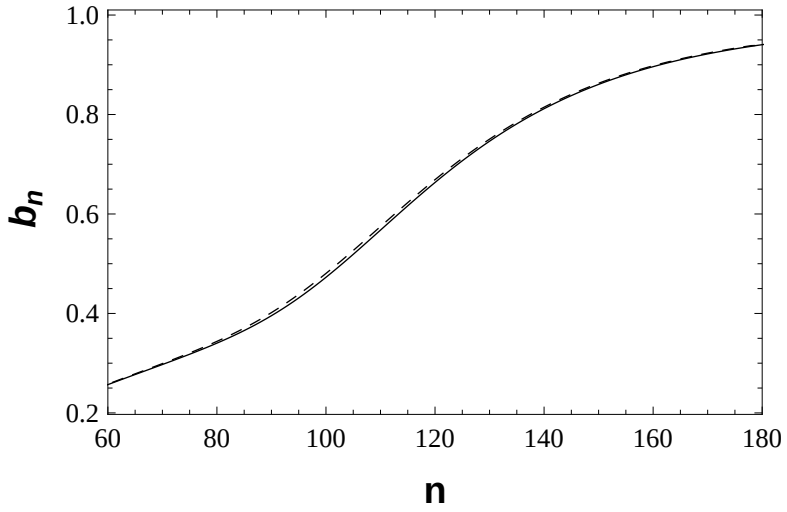

Figure 6.6 – Departure coefficients for a nebula at $T_e = 300\,\mathrm{K}$ with $N_e = 10\,\mathrm{cm}^{-3}$, assuming Case B. Results for a C^3 model is represented by the solid line. The dashed line represents the departure coefficients for the same nebula permeated by an undiluted 3 K blackbody.

general the b_n values were altered on average by 0.2 % and at most by an average of 0.6 %.

Fig. 6.6 shows an example of the effect of the CMBR on the population structure of a cool, low-density cloud. The solid line shows the level populations when no radiation field is present and the dashed line shows how the level populations are changed when a 3 K blackbody field is introduced. The largest deviation for the case shown in Fig. 6.6 is 1.7 %. From these results it is concluded that the CMBR can have a small effect on the departure coefficients. This effect will be more pronounced at larger redshifts and should therefore be included in future models.

6.3.3 Bremsstrahlung

Continuum radiation from HII regions is a combination of thermal emission from dust within the nebula and free-free emission from the unbound particles in the nebula. The free-free transitions occur predominantly due to the acceleration of free electrons in the Coulomb field of positive ions. There are three processes whereby free-free transitions can occur, analogous to the processes for bound-bound and bound-free transitions. Spontaneous emission from free-free transitions is the dominant free-free process and radiation produced by this process is known as bremsstrahlung.

The free levels are not quantized like the bound levels, so bremsstrahlung has a continuous spectrum.

The aim of this part of the study was to get a crude estimate of the effect that bremsstrahlung might have on the departure coefficients, in particular RRLs. A rough second-order fit was done to the Bremsstrahlung data presented in Gordon & Sorochenko (2002) for the HII region W3. The model was run with a radiation field described by

$$J_\nu^B = 10^{-23}\left(-3\times10^{-22}\nu^2 + 3\times10^{-11}\nu + 2\right)$$

where J_ν^B is in cgs units.

It was found the the the effect of J_ν^B on the departure coefficients is negligible. Even with $10^5 J_\nu^B$, the effect on the departure coefficients is minimal ($< 0.3\,\%$). This is consistent with the work of Dyson (1969), who found that the effects of free-free radiation on the b_n values are negligible.

Chapter 7

Escape Probability of Lyman Photons

7.1 Background to the Problem

When investigating the Balmer decrement in diffuse nebulae, Zanstra (1927) argued that all Lyman radiation would be degraded to Lyα radiation which alone would be able to escape the nebula. Baker & Menzel (1938) later formalized his argument into two possible situations of nebular extinction, namely Case A and B. Under Case B it is assumed that a Lyman photon in the nebula is absorbed very close to the point where it was generated and does not escape from the nebula. Therefore, the nebula is optically thick to Lyman line radiation. Case A assumes that the nebula is optically thin to all line radiation.

This distinction is warranted when one considers the population of the ground state in comparison to the populations of excited states. The rate at which valence electrons cascade down to the ground state is much faster than the rate of transitions from the ground state. This means that almost all of the neutral hydrogen in a nebulae is in the ground state and the population of the ground level is therefore much larger that the population of any other level. The mean free path of a line photon depends inversely on the population of the lower level (see discussion below in § 7.2), so the mean free path of Lyman photons are much smaller than that of other line photons. In an HII region with density $10^3\,\mathrm{cm}^{-3}$ at $10^4\,\mathrm{K}$ the mean free path of a Lyα photon is of the order of $10^{-15}\,\mathrm{pc}$. This is very much smaller than

the size of a typical HII region (1 to 50 pc) and it can be assumed that the photon is absorbed very close to the spot where it is emitted.

Case B implies that the rate of absorptions from the ground state is counterbalanced by the transitions to the ground state. Therefore all transitions from and to the ground state may be neglected and the sums in the rate equation (3.1.5) are done from $n = 2$, and not from $n = 1$ as for Case A. Baker & Menzel (1938) found calculations assuming Case B to be in better agreement with observations than for Case A. Aller (1951) confirmed this by studying a number of planetary nebulae. Osterbrock (1962) concluded that Case B is a good quantitative approximation. All three of these investigations were performed for transitions with $n \leq 35$.

The observational success of Case B in the optical regime has resulted in it being taken for granted that Case B applies for calculations involving high n levels without reconsidering the physics involved. The discussion in § 7.2 shows that the mean free paths of line photons depend inversely on the Einstein A-values of the transition that produced the photon. Lyman lines from high n levels have much smaller A-values than Lyman lines from low levels ($A_{21} = 4.7 \times 10^8\,\mathrm{s}^{-1}$, whereas $A_{1101} = 7.8 \times 10^{-1}\,\mathrm{s}^{-1}$), which implies that their mean free path will be much larger. If the mean free path is in the order of the dimensions of the HII region, a typical high Lyman photon will be able to escape from the nebula and Case B will not be applicable.

The difference between Case A and B might appear irrelevant when considering Fig. 7.1 for very high energy levels, since the difference between the b_n values for the two cases becomes small for high n. But Goldberg (1966) showed that small differences between departure coefficients become important at high principal quantum numbers, particularly for RRLs, which deal exclusively with transitions between high n levels. For a HII region at $T_e = 10^4\,\mathrm{K}$, $b_{110} - b_{109} = 7 \times 10^{-4}$ which is large compared to $h\nu/kT_e = 2.40 \times 10^{-5}$. Neglecting small departures from LTE will greatly underestimate the amount of stimulated emission.

It is necessary to investigate the mean free path of Lyman photons from energy levels with large principal quantum numbers to ascertain whether Case B is valid for these transitions as well, or if it is required to create a hybrid case where Case A applies for small n and Case B to large n.

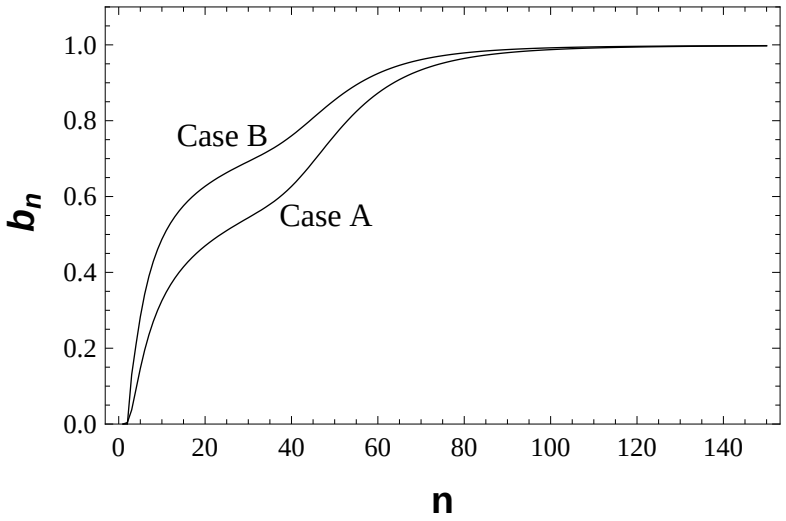

Figure 7.1 – Departure coefficients for the same nebula with $N_e = 10^4\,\mathrm{cm}^{-3}$ and $T_e = 10^4\,\mathrm{K}$ assuming Case A and Case B. A calculation assuming Case B disregards all transitions to and from level $n = 1$, where Case A allows for transitions to and from all levels.

7.2 Mean Free Path of a Lyman Photon

To be able to investigate whether Case B is a valid assumption for Lyman transition from high energy levels, the mean free path of such a photon needs to be calculated. If the mean free path is in the order of the size of the nebula, such a photon will typically escape the nebula and Case B will not be valid. The mean free path of a photon is given by

$$l_\nu = \frac{1}{\kappa_\nu} \tag{7.2.1}$$

where κ_ν is the extinction coefficient or opacity. The extinction coefficient is a macroscopic quantity that gives a measure of the rate of decrease of intensity as radiation passes through a medium.

The optical depth is given by

$$\tau_\nu(s) = \int_0^s \kappa_\nu(s')\,ds'$$

where ds' is measured along the path of the radiation. A medium is said to be optically thick if $\tau_\nu > 1$ and optically thin if $\tau_\nu < 1$. A typical photon can escape from the medium if it is optically thin.

In terms of the Einstein coefficients, the extinction coefficient for a transition be-

tween level n and level n' with $n' < n$ is given by

$$\kappa_\nu = \frac{h\nu}{4\pi}\left(N_{n'}B_{n'n} - N_n B_{nn'}\right)$$

where ν is the frequency associated with the transition. This can be written as

$$\kappa_\nu = \frac{h\nu}{4\pi}N_{n'}B_{n'n}\left(1 - \frac{N_n}{N_{n'}}\frac{B_{nn'}}{B_{n'n}}\right).$$

Substituting the Einstein relation (2.1.2) and the Boltzmann distribution corrected for non-LTE conditions (3.1.2) into the above equation gives

$$\kappa_\nu = \frac{h\nu}{4\pi}N_{n'}B_{n'n}\left(1 - \frac{b_n}{b_{n'}}e^{-h\nu/k_BT}\right).$$

Using the Einstein relation (2.1.1) this can be written as

$$\kappa_\nu = \frac{c^2}{8\pi\nu^2}\left(\frac{n}{n'}\right)^2 N_{n'}A_{nn'}\left(1 - \frac{b_n}{b_{n'}}e^{-h\nu/k_BT}\right). \tag{7.2.2}$$

Substituting for $N_{n'}$ the population of level n' in (7.2.2) using the Saha-Boltzmann equation (3.1.1) gives

$$\kappa_\nu = \frac{c^2}{8\pi\nu^2}\left(\frac{h^2}{2\pi m_e k_B T_e}\right)^{3/2}\exp\left(\frac{\chi_{n'}}{k_BT_e}\right)N_eN_ib_{n'}n^2A_{nn'}\left(1 - \frac{b_n}{b_{n'}}e^{-h\nu/k_BT}\right). \tag{7.2.3}$$

The mean free path of a Lyman photon is obtained by setting $n' = 1$ in (7.2.3) and using (7.2.1).

In order to use (7.2.3), the departure coefficient of the ground state b_1 needs to be known. The model described in § 3.1 is not suited to calculate b_1, and another argument was used.

The densities of the electrons, protons and and neutral hydrogen atoms are related by the fraction of neutral hydrogen ξ. Let N_H be the number density of the total amount of hydrogen in the plasma and N_{H^0} the number density of the neutral hydrogen atoms, then

$$\begin{aligned} N_H &= N_{H^0} + N_i \\ N_{H^0} &= \xi N_H \qquad (7.2.4) \\ N_e = N_i &= (1-\xi)\,N_H\,. \qquad (7.2.5) \end{aligned}$$

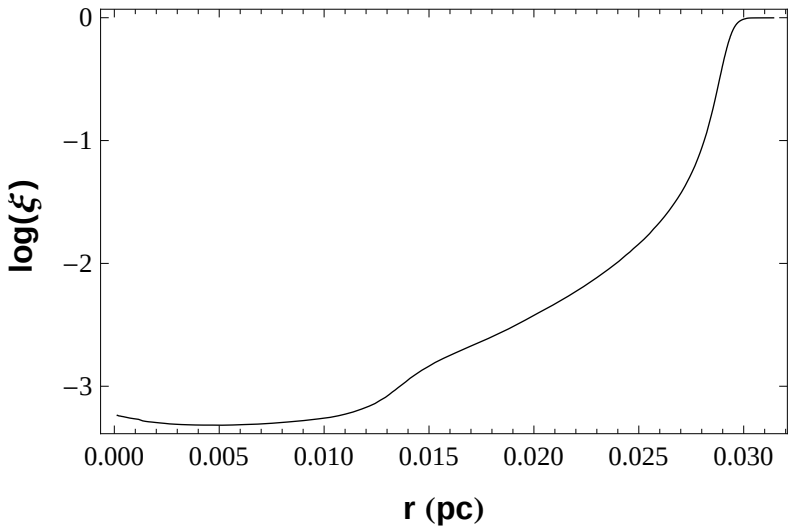

Figure 7.2 – The neutral hydrogen fraction for a spherically symmetric planetary nebula as a function of radial distance (starting at 10^{17}cm) from a central ionizing blackbody source at $T = 150\,000\,\mathrm{K}$ with a radius of 10 km.

The hydrogen neutral fraction is defined such that if $\xi = 0$, the plasma is fully ionized so that $N_e = N_i = N_H$ and if $\xi = 1$, the plasma is completely neutral so that $N_{H^0} = N_H$ and $N_e = N_i = 0$. Substituting (7.2.4) into (7.2.5) gives

$$N_{H^0} = \frac{\xi}{1-\xi} N_e \,.$$

As discussed in § 7.1, almost all of the neutral hydrogen atoms will have their electron in the $n = 1$ state, so that $N_1 \approx N_{H^0}$.

For an astrophysical plasma that is ionized by a central source, like a planetary nebula, the region closest to the source will be almost completely ionized. This ionized region will be surrounded by a neutral region if the gas is larger than the mean free path of the ionizing photons. The transition region between the ionized and neutral regions tend to be small so that ξ is either small or approaches 1. The neutral fraction as a function of distance from a central star is shown in Fig. 7.2. A typical value for ξ in the ionized region is between 10^{-6} and 10^{-3} (Osterbrock & Ferland, 2006).

The number density of electrons in the ground state under conditions of TE N_1^* is given by the Saha equation

$$N_1^* = N_e N_i \left(\frac{h^2}{2\pi m_e k_B T_e} \right)^{3/2} \exp\left(\frac{\chi_1}{k_B T_e} \right) . \tag{7.2.6}$$

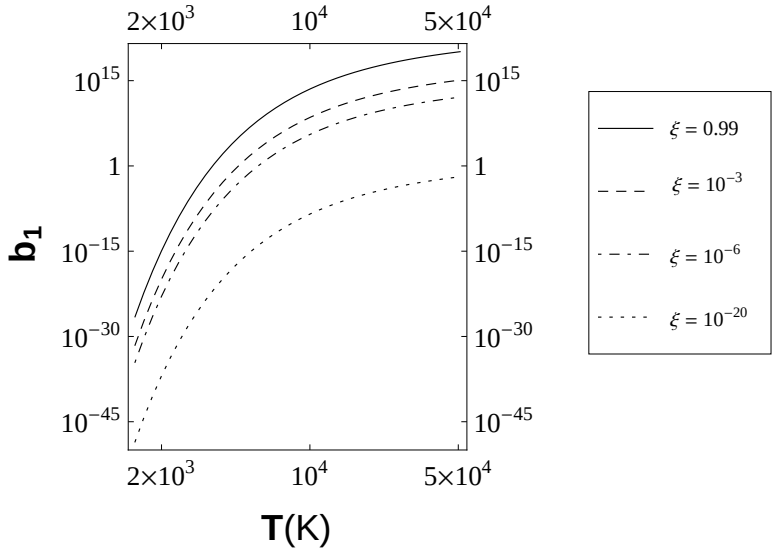

Figure 7.3 – The departure coefficient of the ground state of hydrogen for a plasma with $N_e = 10^3\,\mathrm{cm}^{-3}$ as a function of electron temperature. Plots are shown for various hydrogen neutral fractions.

The actual number density of atoms in the ground state is given by the corrected Saha-Boltzmann equation (3.1.1)

$$N_1 = b_1 N_e N_i \left(\frac{h^2}{2\pi m_e k_B T_e}\right)^{3/2} \exp\left(\frac{\chi_1}{k_B T_e}\right) . \tag{7.2.7}$$

The departure coefficient of the ground level $b_1$can then be calculated by dividing (7.2.7) by (7.2.6). This gives

$$\begin{aligned} b_1 &= \frac{N_1}{N_1^*} \\ &= \frac{\xi}{1-\xi}\frac{N_e}{N_1^*} \end{aligned}$$

The mean free path of Lyman photons can be evaluated by calculating the extinction coefficient using (7.2.3) and putting it into (7.2.1). The results for a typical ionized region ($\xi = 10^{-4}$) are shown in Fig. 7.4. The temperature dependence of the mean free path is very weak, so all results shown are for $T_e = 10^4\,\mathrm{K}$. The departure coefficients that were used in the calculation were calculated assuming Case A, so that b_2 could be calculated, with no ionizing radiation field. This does not affect

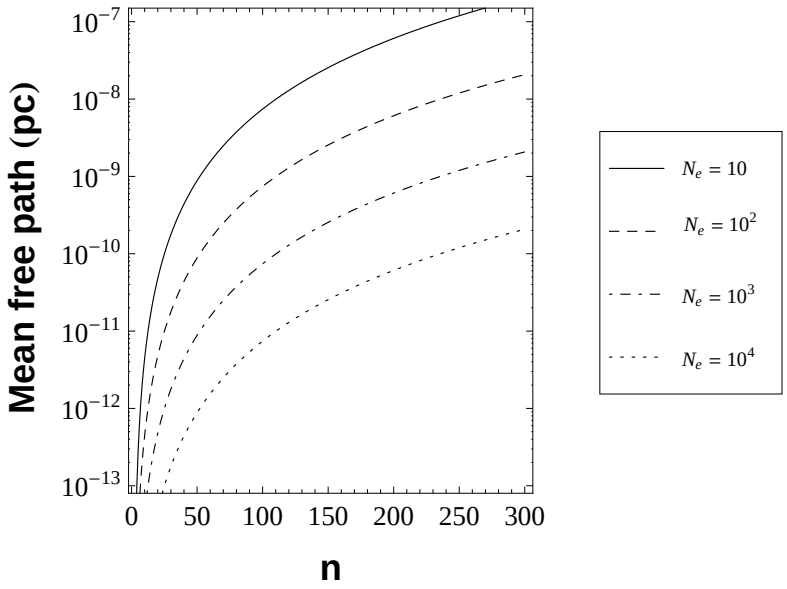

Figure 7.4 – The mean free path of Lyman photons in parsecs with respect to the upper n level for various free electron densities. The mean free path has a weak dependence on temperature, so all values shown are for $T_e = 10^4\,\mathrm{K}$ and $\xi = 10^{-4}$.

the results as the actual values of b_n for $n \geq 2$ used in (7.2.3) has very little effect on the mean free path.

It is clear from Fig. 7.4 that the the mean free path of Lyman photons under conditions typical to gaseous nebulae is always very small compared to the size of the nebula, even for Lyman transitions from high n levels. Therefore, Case B is a valid assumption for all lines from typical gaseous nebulae.

In principle, it is possible to set up conditions where Case A will be appropriate for high Lyman lines. Fig. 7.5 shows the mean free path of various Lyman photons as a function of the neutral hydrogen fraction ξ. The mean free path of the high Lyman photons do become large at very low values of ξ. Suppose $\xi = 10^{-14}$ in a plasma with $N_e = 10^2\,\mathrm{cm}^{-3}$. Then there will be $\xi N_e = 10^{-12}$ neutral particles per cubic centimetre, that is 1 neutral particle for every $10^6\,\mathrm{m}^3$. This means that the free electrons almost never recombine, and a recombination spectrum will not be observable from the plasma and Case A and Case B will be irrelevant.

It should be noted that this treatment does not consider the Doppler broadening of the lines and the results are preliminary. The mean free path of photons will increase if Doppler broadening were considered, but not enough to invalidate the

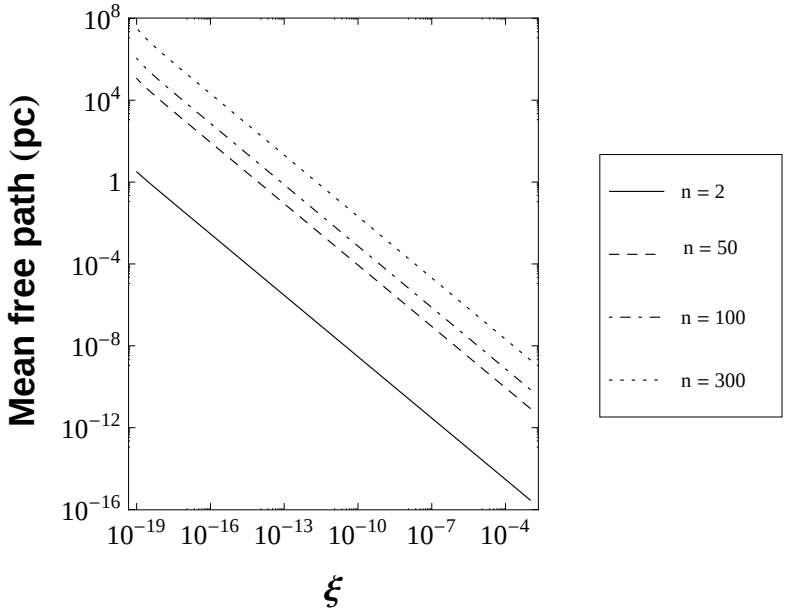

Figure 7.5 – Mean free path of Lyman photons from various energy levels as the neutral hydrogen fraction ξ changes for a plasma with $T_e = 10^4\,\mathrm{K}$ and $N_e = 10^2\,\mathrm{cm}^{-3}$. The mean free path of Lyman photons from low levels always remain small, but for $\xi \ll 1$ Case A is more suitable for high Lyman lines.

main results. Once the model has been upgraded to consider the angular momentum levels explicitly, the escape probabilities will be looked at more carefully.

Chapter 8

Conclusion

8.1 Discussion

A comprehensive model for calculating the n-method populations of a pure hydrogen plasma has been presented. It has been assumed that the nebula is homogeneous, unbounded and permeated by a constant radiation field. Departure coefficients for bound energy levels were computed by accounting for all radiative and collisional processes, bound-bound and bound-free, via all possible transition routes. The model is comparable with the most definitive models available at present (see Salem & Brocklehurst, 1979).

The theory and methods used in the calculations have been discussed in detail. A full quantum mechanical treatment has been used to calculate the probability of processes occurring, so that the atomic data is very accurate. Modern computing power also allowed all of the calculations to be performed in double precision to improve accuracy. The collisional processes introduced the most inaccuracy into the calculations, as the collisional processes are three-body processes and are solved non-analytically. Another factor responsible for errors is small numerical errors that are introduced because of the complexity of the calculations. This difficulty can be overcome by introducing more advanced numerical programming methods into the program.

Because of the collisional cross-sections that were used, the code is valid for a larger range of temperatures than any of the current models. Because the parameters for

astronomical plasmas vary greatly, this broadens the code's potential for modelling a variety of astronomical environments,. Nova shells with electron temperatures $T_e < 1\,000\,\mathrm{K}$ have been detected (Williams et al., 1978), while supernova remnants have temperatures of about $10^6\,\mathrm{K}$.

The results from the model developed in this work were compared to previous calculations and found to be in good agreement. Discrepancies are small and can be explained by the different methods used to calculate atomic transition probabilities and to handle numerical and computational challenges. One of the objectives of this project was to check for systematic errors in previous calculation by independently developing code. No such errors were found.

A preliminary investigation of the effects of an external radiation field on the departure coefficients was done. In principle the external radiation field should be included in the calculations of b_n values, but the incorporation of a radiation field into such a model is not trivial and it necessitates that the geometry of the system be taken into account. It was found that the ionizing radiation from a nearby star can have a significant effect on the departure coefficients of high n levels, as can the CMBR. The effects of free-free emission on the b_n values were found to be insignificant.

For the conditions considered in this work, the departure coefficients always increase monotonically with n. Therefore, no lines will be amplified and maser action will not be observed. Even though the conditions for RRL masers are stringent, they are possible and have been observed (Strelnitski et al., 1996).

The problem of whether or not to include Lyman transitions in the calculations when determining departure coefficients was investigated. The mean free path of Lyman photons from the different energy levels was investigated under various environmental conditions. It was concluded that the escape probability of Lyman photons are negligibly small for conditions found in astronomical plasmas that produce a recombination spectrum. Therefore, it is always appropriate to assume Case B when determining departure coefficients.

8.2 Future Work

This project has a lot of potential to be developed further into a sophisticated model with a wide range of applications. The code has been written with this in mind to

facilitate future extensions.

The first improvement that will be made is to upgrade the model to an nl-model that explicitly calculates the populations of the angular momentum levels, as opposed to assuming that they are statistically populated. The n-model constructed in this work was the first step towards this, as the nl-model will resolve the angular momentum levels by an iterative procedure that requires b_n values as initial values. This will then be the first nl-model that takes the external radiation field into account.

An important step will be to extend the model from considering a pure hydrogen nebula to a mixture of helium and some metals, which is a more physically consistent situation in astronomical environments. The hydrogenic model serves as the basis for all other atoms, so the ground work for this has already been done.

It has become clear from this project that one has to be very careful with the numerical methods that one employs is such a code. The numerical methods used in this work will be reviewed and refined to increase the precision of the results.

Preliminary analysis of the effects of an external radiation field on the departure coefficients was done in this work. To investigate the full consequences of the radiation field, the code will be extended to a photoionization code that incorporates radiative transfer through the plasma. This will involve a finite element-kind of calculation to determine how the radiation changes as it propagates through the nebula. This means that the diffuse radiation field emitted by the nebula itself can also be incorporated into the model.

The photoionization code will consider the physical as well as the ionization structure of the nebula, as opposed to the infinite and homogeneous case regarded in this work. It is important to take geometrical factors into account, as this will determine what radiation escapes from the nebula and can be observed. Once this is completed, rudimentary assumptions like Case A and Case B will be obsolete as the radiative transfer model will account for escape probabilities explicitly.

The spectrum of the radiation that permeates the nebula in the model will also be more sophisticated. The ionizing spectrum will be improved from a blackbody spectrum to a stellar spectrum. This work has shown that the CMBR can affect the departure coefficients, so this radiation needs to be included in the calculations. This effect would be more pronounced if one considers objects at a higher redshift, where the temperature of the CMBR is higher. The effect of bremsstrahlung was

found to be insignificant, but the inclusion of the radio continuum into the model is important when interpreting RRLs, as the radio continuum will be underlying these lines. The thermal emission from dust in the nebula also forms part of the radio continuum and will be included in future models.

Once these improvements are made, the applicability of the model will be very wide. It will be able to model interesting environments which have not been looked at before in the radio regime. These include hydrogen deficient nebulae, supernova remnants and shock fronts. Hydrogen deficient knots can form in planetary nebulae and have not been modelled. In supernova remnants, the radiation field is due to synchrotron radiation and the effects of this have not yet been studied in the radio regime. Shock fronts can also ionize gas, as is the case in Herbig-Haro objects. These are small, dense nebulae in star forming regions that are created when ejected material from a newborn star collides with interstellar gas.

Future models will extend our understanding of gaseous nebulae and prove to be a valuable asset to radio astronomy in general. The quality of radio observations will enter a new era with groundbreaking instruments like the SKA, MeerKAT and ALMA. Flexible and accurate theoretical models are needed, to enable the interpretation of these observations as they become available.

Bibliography

Abramowitz, M. & Stegun, I. A. 1972, Handbook of Mathematical Functions, ed. Abramowitz, M. & Stegun, I. A.

Aller, L. H. 1951, ApJ, 113, 125

Baker, J. G. & Menzel, D. H. 1938, ApJ, 88, 52

Bauman, R. P., Porter, R. L., Ferland, G. J., & MacAdam, K. B. 2005, ApJ, 628, 541

Bohm, D. & Aller, L. H. 1947, ApJ, 105, 131

Brocklehurst, M. 1970, MNRAS, 148, 417

Brocklehurst, M. 1971, MNRAS, 153, 471

Brocklehurst, M. & Salem, M. 1977, Computer Physics Communications, 13, 39

Burgess, A. 1958, MNRAS, 118, 477

Burgess, A. 1965, MmRAS, 69, 1

Burgess, A. & Seaton, M. J. 1960, MNRAS, 120, 121

Burgess, A. & Summers, H. P. 1969, ApJ, 157, 1007

Burgess, A. & Summers, H. P. 1976, MNRAS, 174, 345

Caswell, J. L. & Haynes, R. F. 1987, A&A, 171, 261

Downes, D., Wilson, T. L., Bieging, J., & Wink, J. 1980, A&AS, 40, 379

Dyson, J. E. 1969, ApJ, 155, 47

Einstein, A. 1916, Deutsche Physikalische Gesellschaft, 18, 318

Gee, C. S., Percival, L. C., Lodge, J. G., & Richards, D. 1976, MNRAS, 175, 209

Goldberg, L. 1966, ApJ, 144, 1225

Gordon, M. A. & Sorochenko, R. L., eds. 2002, Astrophysics and Space Science Library, Vol. 282, Radio Recombination Lines. Their Physics and Astronomical Applications

Gordon, W. 1929, Ann. der Phys., 2, 1031

Hoang-Binh, D. 1968, ApL, 2, 231

Hummer, D. G. & Storey, P. J. 1987, MNRAS, 224, 801

Inokuti, M. 1971, Reviews of Modern Physics, 43, 297

Kardashev, N. S. 1959, SvA, 3, 813

Karzas, W. J. & Latter, R. 1961, ApJs, 6, 167

Menzel, D. H. 1937, ApJ, 85, 330

Milne, E. A. 1924, Phil Mag, 47, 209

Osterbrock, D. E. 1962, ApJ, 135, 195

Osterbrock, D. E. & Ferland, G. J. 2006, Astrophysics of gaseous nebulae and active galactic nuclei, ed. Osterbrock, D. E. & Ferland, G. J.

Pengelly, R. M. 1964, MNRAS, 127, 145

Peters, W. M., Lazio, T. J. W., Clarke, T. E., Erickson, W. C., & Kassim, N. E. 2011, A&A, 525, A128

Plaskett, H. H. 1928, Harvard College Observatory Circular, 335, 1

Reifenstein, E. C., Wilson, T. L., Burke, B. F., Mezger, P. G., & Altenhoff, W. J. 1970, A&A, 4, 357

Rodríguez-Rico, C. A., Goss, W. M., Turner, J. L., & Gómez, Y. 2007, ApJ, 670, 295

Roy, A. L., Goss, W. M., & Anantharamaiah, K. R. 2008, A&A, 483, 79

Roy, A. L., Oosterloo, T., Goss, W. M., & Anantharamaiah, K. R. 2010, A&A, 517, A82

Salem, M. & Brocklehurst, M. 1979, ApJS, 39, 633

Seaton, M. J. 1959, MNRAS, 119, 90

Seaton, M. J. 1964, MNRAS, 127, 177

Sejnowski, T. J. & Hjellming, R. M. 1969, ApJ, 156, 915

Smits, D. P. 1991, MNRAS, 248, 193

Sorochenko, R. L. & Borodzich, É. V. 1966, Soviet Physics Doklady, 10, 588

Stepkin, S. V., Konovalenko, A. A., Kantharia, N. G., & Udaya Shankar, N. 2007, MNRAS, 374, 852

Storey, P. J. & Hummer, D. G. 1995, MNRAS, 272, 41

Strelnitski, V. S., Ponomarev, V. O., & Smith, H. A. 1996, ApJ, 470, 1118

Vriens, L. & Smeets, A. H. M. 1980, PhRvA, 22, 940

Williams, R. E., Woolf, N. J., Hege, E. K., Moore, R. L., & Kopriva, D. A. 1978, ApJ, 224, 171

Wilson, T. L., Mezger, P. G., Gardner, F. F., & Milne, D. K. 1970, A&A, 6, 364

Zanstra, H. 1927, ApJ, 65, 50